Soil Dynamics and Earthquake Engineering 152 (2022) 107036

Contents lists available at ScienceDirect

Soil Dynamics and Earthquake Engineering

journal homepage: www.elsevier.com/locate/soildyn

Influence of the sloping ground conditions and the subsequent shaking events on the pile group response subjected to kinematic interactions for a liquefiable sloping ground

Anurag Sahare [a,*], Kyohei Ueda [b], Ryosuke Uzuoka [b]

[a] Graduate School of Engineering, Kyoto University, Kyoto daigaku-katsura, Nishikyo-ku, Kyoto, 615-8530, Japan
[b] Disaster Prevention Research Institute, Kyoto University, Gokasyo, Uji, Kyoto, 611-0011, Japan

ARTICLE INFO

Keywords:
Centrifuge model test
Soil-pile interaction
Kinematic interaction
Lateral spreading
Soil liquefaction

ABSTRACT

The soil-pile kinematic interaction under large nonlinearity, including soil liquefaction, represents a complex phenomenon that depends on many unforeseen factors. This paper presents the results of dynamic centrifuge tests carried out considering varying sloping inclination angles for a liquefiable ground subjected to four successive earthquake shakings having an increasing amplitude of acceleration. The results indicated the ground surface sloping inclinations to have a significant influence on the kinematic bending moment response of the piles. The significantly larger kinematic moments were generated on the downslope pile compared to the upslope pile highlighting the non-existence of shadowing effects during the lateral spreading for a liquefiable sloping ground. The kinematic moments generated during the first shaking, having predominant lateral spreading were substantially larger than the following three shakings, indicating the complex kinematic interaction to depend not only on the amplitude of base excitation; but mostly on the magnitude of lateral spreading. Moreover, the influences of the generated E.P.W.P on the pile response was studied and it was found that the piles may receive maximum kinematic moments around the occurrence of liquefaction to the time of initiation of dissipation phase of the generated E.P.W.P.

1. Introduction

1.1. Background

Earthquake-induced soil liquefaction & lateral spreading may result in extensive damage to the soil-structure systems and remains a major threat among geotechnical earthquake engineering community. Availability of case history databases, centrifuge & 1-g shake table testing results and the use of sophisticated constitutive models has led to the understandings about key mechanisms during this phenomenon [1–9]. The performance of a pile foundation during the liquefaction-induced lateral spreading has been a major concern due to the 1964 Niigata, 1989 Loma-Prieta, 1995 Kobe earthquake, and more recently during the 2010–2011 Canterbury earthquake sequence, which caused widespread damage to the pile foundations [10–14]. During an earthquake, the piles are subjected to a combined loading arising from the inertial (due to superstructure) and kinematic interactions from the surrounding soil. The kinematic interactions involving the pile foundation due to the lateral spreading of soil represents a complex soil-pile interaction phenomenon which involves the degradation and a loss in the shear strength of soil due to the generation of excess pore pressure. Fujii et al. [15] and Uzuoka et al. [16] showed the cracking or failure was not only limited near the pile head but was also observed near the lower section of the pile during the 1995 Kobe earthquake, indicating the pile's mechanical behavior is governed by both the inertial and kinematic interaction with the surrounding soil. This may be even more problematic or would represent a more complex phenomenon under the presence of strong nonlinearity, including the occurrence of soil liquefaction deep near the lower segment of pile, where the kinematic forces are predominant. Hence, it is important to study the kinematic bending response of piles under such strong nonlinearity existing throughout the depth of soil model. For such cases, ignoring the contribution of the surrounding soil to the pile surface might result in an unsafe design with the possible failure involving the formation of plastic hinges near the lower section of the pile.

Over the years, significant research has been carried out to study the

* Corresponding author.
E-mail address: sahare.rahul.84a@st.kyoto-u.ac.jp (A. Sahare).

https://doi.org/10.1016/j.soildyn.2021.107036
Received 16 November 2020; Received in revised form 16 September 2021; Accepted 13 October 2021
Available online 27 October 2021

pile foundation response during an earthquake induced liquefaction. Abdoun et al. [17] examined the single and group pile's response to earthquake induced liquefaction and subsequent lateral spreading involving multi-layer soil models using a laminar box. They found the maximum moments to occur at the interface of liquefiable and non-liquefiable soil layers. Further, these moments were found to initially increase followed by a decreasing response, although the free field soil displacement showed a continued rise till the end of shaking, indicating significant softening of soil after a few cycles of earthquake loading due to predominant liquefaction. Uzuoka et al. [18] investigated the damage process of a pile group foundation supporting a five-story building in reclaimed land during the 1995 Kobe earthquake using a 3-D soil-water-coupled numerical analysis. They showed the inertial effects to be predominant throughout the length of pile, leading to the yielding of piles with large horizontal displacements recorded by the building before the occurrence of soil liquefaction during the initial stage of loading. However, following the soil liquefaction throughout the depth of reclaimed land, kinematic interaction is apparent near the bottom of reclaimed land. Motamed and Towhata [19] carried out 1-g shaking table tests for a 3X3 pile group behind a sheet pile quay wall subjected to liquefaction induced large ground deformations and found the lateral forces experienced by the pile to vary depending on the positions of the pile in a group. Motamed et al. [20] investigated the response of pile group subjected to liquefaction induced lateral spreading using 1-g shake table tests. They examined the influences of various parameters on the pile group response, which included earthquake characteristics and soil conditions. The findings included the dependency of the lateral displacement on the amplitude, frequency and direction of shaking. Moreover, the authors concluded the front and the rear piles in a group to receive larger amount of lateral forces, which was shown to depend on the motion of the liquefied soil during shaking. Haeri et al. [21] showed the lateral soil pressure exerted on the piles during a lateral spreading depends on the location of a pile within a group, which in turn depends on the shadowing and neighboring effects.

Motamed et al. [22] conducted large scale shake table testing using E-Defense facility for a pile group located close to quay wall subjected to liquefaction-induced lateral spreading. Large ground flow tilted the superstructure towards the water side along with substantial damage to the piled-foundations because of large soil displacements near waterside, which decreased towards landside. Liu et al. [23] conducted a series of centrifuge model tests for a 4 x 4 pile group in liquefiable soils considering bidirectional shaking for the first time. They showed the internal piles subjected to greater bending moments, the mechanism of which is explained with the help of lateral soil forces and pile deflection along the depth. At the same time, they also studied the seismic response of a pile group under the superstructure-pile inertial interaction and without superstructure, thus considering only the kinematic part. Their study highlights the dominant influence of the soil-pile kinematic interactions in the liquefiable ground. Ebeido et al. [24] carried out 1-g shake table experiments and found the maximum bending moment to occur during the initial stages of loading as the soil liquefies. Xu et al. [25] carried out large scale shaking table tests to study the seismic behavior of pile group subjected to inertial and kinematic interactions in liquefiable and non-liquefiable soil. Based on the experiments, they observed differed responses for piles subjected to the same earthquake loading depending on whether they are installed in liquefiable or non-liquefiable soil strata, with significantly larger bending moments being recorded in the liquefiable site, although the liquefiable soil degraded more considerably than the non-liquefiable strata.

1.2. Motivation and objectives of the present study

Although, the previous studies have certainly improved the understanding of the pile response to lateral spreading; apart from the 1-G shake table tests by Motamed et al. [20], no qualitative study has been carried out to consider the influences of sloping inclinations of the ground surface; especially considering a larger prototype dimensions. This is an important practical issue, because the foundation systems may be subjected to different kinematic interactions with the surrounding soil during an earthquake, which may strongly depend on the sloping inclinations of the ground surface. This may in turn influence the lateral deformation mechanism of the piles and can lead to the piles experiencing different magnitude of kinematic bending moments. Barlett and Youd [26] for the first time developed empirical equations for predicting lateral displacement based on Japan and U.S. case histories which resulted in liquefaction-induced lateral spread. They found the horizontal displacement to statistically correlate with the inclination of the ground surface during a lateral spreading. Apart from that, Youd et al. [27], Gillins et al. [28] presented the empirical equations to evaluate the lateral displacement due to liquefaction induced lateral spreading, for which one of varying parameters was the ground slope. Although, these studies did not focus on the soil-structure interactions, yet they revealed the complex lateral displacement mechanism of the soil to depend on the sloping inclinations of the ground surface during a lateral spreading event. Hence, it is important to assess the influence of variability of the sloping inclinations of the ground surface by evaluating the soil-pile kinematic interactions during a liquefaction induced lateral spreading based on different ground slopes.

At the same time, limited comprehensive studies have been carried out to consider the influences of the generated excess pore pressure on the maximum kinematic moment response of the group piles near the bottom section of a soil model, where the kinematic forces are predominant. This is an important issue for cases involving the presence of strong non-linearity including the occurrence of soil liquefaction towards the bottom section of piles, and to assess the potential influence of the loss in stiffness and shear strength of the surrounding soil on the pile response. In the past [25] have shown the degraded liquefied soil to impart significantly larger moments. Hence, it would be of use to analyze the kinematic moment demands experienced by the pile through the earthquake loading phase depending on the excess pore pressure build up and dissipation. The authors also feel the need for a rigorous framework to better understand the response and the bending moment demand of the upslope and downslope pile during various loading stages under different kinematic interactions.

To establish the influence of the ground surface sloping inclinations under large non-linear conditions with the incremental shaking intensities and to correlate the excess pore pressure buildup and dissipation on the kinematic moment demands of the pile, the authors presented the results of series of two centrifuge experiments in this paper. A brief explanation about the geotechnical centrifuge at the Disaster Prevention Research Institute (DPRI), Kyoto University, and the experimental procedure is described in Section 2. The experimental results in the form of acceleration responses, free field and far field excess pore pressure response, lateral soil displacement, velocity time history responses of the liquefied soil, lateral soil pressure responses and the Fourier amplitude responses evaluated at the pile head are shown in Section 3. Section 4 shows the influence of the generated E.P.W.P on the maximum kinematic moment response of the upslope and downslope pile during an earthquake loading. Section 5 shows the kinematic bending moment response for the pile system (upslope and downslope pile), emphasizing the maximum and residual kinematic moments. Section 6 explains the response of pile foundation in terms of maximum monotonic bending moments experienced by the upslope and downslope pile during the different shaking events.

2. Experimental program

2.1. Centrifuge facility

The centrifuge facility at DPRI was used to carry out the centrifuge model tests. The geotechnical beam-type centrifuge has an effective radius of 2.5 m with a payload capacity of 24 g-ton and the maximum

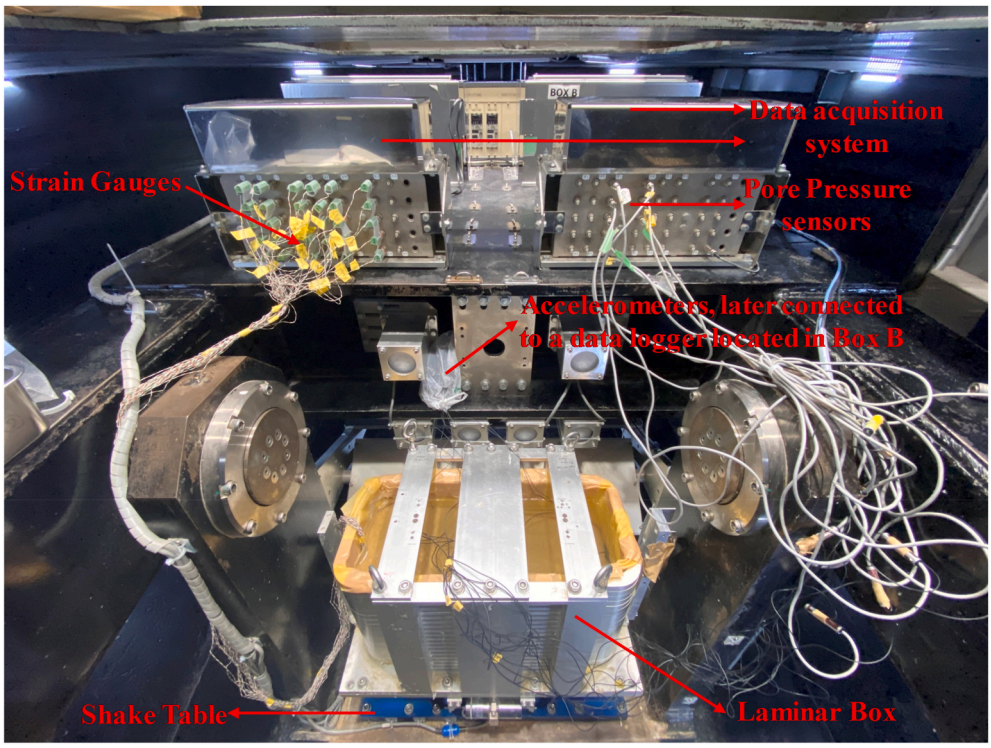

Fig. 1. Experimental Setup for the Centrifuge tests.

reachable centrifugal acceleration of 200g for static and 50g for dynamic tests. The applied shaking direction was parallel to the arm of rotation of centrifuge for the two cases studied. The laminar box consisting of 20 layers of aluminum alloy rectangular rings was used for the experiments. The internal dimensions of the box are 500 mm (L) X 200 mm (W) X 320 mm (H). The laminar box used for the present research is capable of reproducing the free field conditions with regard to the lateral spreading of soil and was found to perform better than the hinged-wall-type shear box (Tobita et al. [29]; Bai et al. [30]) primarily because of the large number of laminar rings with considerably lesser friction due to the linear bearings. Fig. 1 shows the laminar box mounted on the shake table before carrying out the experiments. More details about the centrifuge facility at DPRI can be found in Ueda et al. [31].

2.2. Model configurations

Two series of experiments were conducted under a centrifugal acceleration of 50g. Model UL5 and UL10 represent a uniformly liquefiable sloping ground having an inclination of 5° and 10°, respectively. Fig. 2 displays the model configuration in prototype scale for UL5 (top and front view) along with the location of all the sensors and pile arrangement, while Fig. 3 represents the model configuration for UL10. The soil response to shaking was evaluated in terms of excess pore pressure, acceleration time history, lateral displacement and velocity time responses. The soil-pile kinematic interaction was assessed in terms of bending moments evaluated from the strain gauges for upslope and downslope pile as shown in Figs. 2 and 3. Apart from the 4 piles in a 2X2 pile group, a single pile was also installed located far away from the group pile in order to eliminate pile-pile interactions. However, the response of a single pile is neither presented nor discussed in the present paper. It is worth mentioning that the piles were not connected to a pile cap or any sort of structural mass, in an effort to measure the bending moment demands of pile under the influence limited to kinematic loading arising from the surrounding soil.

2.3. Material properties

Toyoura sand (e_{min} =0.600, e_{max} =0.966, G_s =2.635) having a relative density of 40% is used for the centrifuge experiments in the present study. Additional details about the physical properties of Toyoura sand can be found in Koseki et al. [32]. An aluminum alloy solid circular pile having a diameter of 400 mm and a length of 9 m (prototype) was used to fabricate a 2X2 end bearing group pile as shown in Fig. 4. The adopted pile spacing is 2 m in prototype scale. Further details about the physical properties of piles are shown in Table 1.

2.4. Experimental procedure

Accelerometers, AH series (FUJICERA.; type BW21SG2.; supplied by Fuji Ceramics Corporation and SSK Co., Ltd.), including an accelerometer to measure the input response, were installed in Model UL5 and Model UL10. Accelerometer AH1 was fixed to the bottom plate, as shown in Figs. 2 and 3. Pore pressure transducers, PPTs (SSK Co., Ltd.; type P306AV-5 and P306A-2) were installed to examine the free field and near piles pore pressure rise and dissipation under the different shaking events for the two models. Pore pressure transducers were also installed towards the bottom section of soil models, where the kinematic forces are most significant. The piles were heavily instrumented with the strain gauges (produced by Tokyo Measuring Instruments Lab) to record the bending moments under lateral spreading events. Fig. 1 shows the connection of sensors to the data logger box. The piles were rigidly connected to the base plate, which was fixed to the base of the laminar

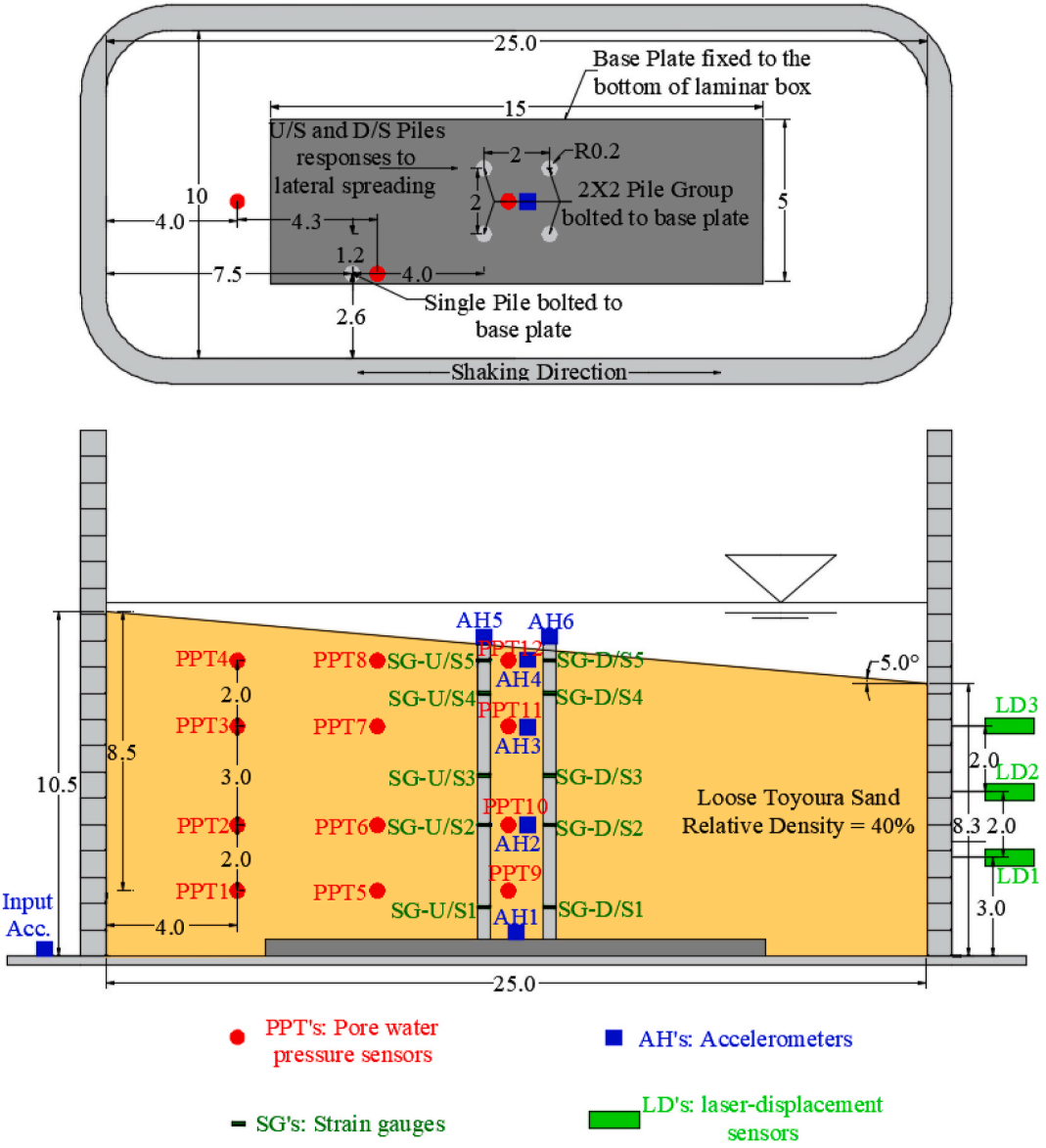

Fig. 2. Test layout for Model UL5 in top and front view (All dimensions are reported in meters in prototype scale); U/S: Upslope Pile and D/S: Downslope Pile.

box as shown in Figs. 2 and 3, to represent a perfectly fixed end pile conditions in a cantilever beam configuration. Toyoura sand was air pluviated to achieve a relative density of 40%. Following the preparation of dry sand, the model in each experiment was saturated using methyl-cellulose solution-Metolose (SM100, supplied by Shin-etsu Chemical Co., Ltd., 1997) prepared to achieve a viscosity of 50 cSt to satisfy the dynamic scaling laws. To saturate the model ground, a vacuum was initially applied following the replacement of air voids with carbon dioxide. Finally, the vacuum pressure was reapplied, and the model specimen was saturated by the continuous drop of the viscous fluid until the water table was raised above the ground surface (on the upslope side) to establish a fully saturated liquefiable soil model specimen under submerged condition. It took around 20–24 h for the complete saturation for both the soil models (UL5 and UL10). Following the saturation process, the laminar box was placed on the shaking table as shown in Fig. 1. The model was gradually spun to reach the desired level of centrifugal acceleration (50g). Once the model specimen reached 50g, a tapered sinusoidal waveform having an excitation frequency of 1 Hz (in prototype scale) was unidirectionally applied using the hydraulic shaker. A series of four successive base excitations in the order of increasing intensity were applied as input motion (hereafter referred to as shaking events (SE)) to examine the model specimen response under different levels of excitation events. Enough time was allowed between the shaking events for the full dissipation of excess pore water pressure generated due to the previous shaking event. Fig. 5 shows the acceleration, arias intensity and 5%-damped spectral accelerations of the four base motions recorded at the bottom of container as an input motion to the two models. From the figure, one can say that both the models were

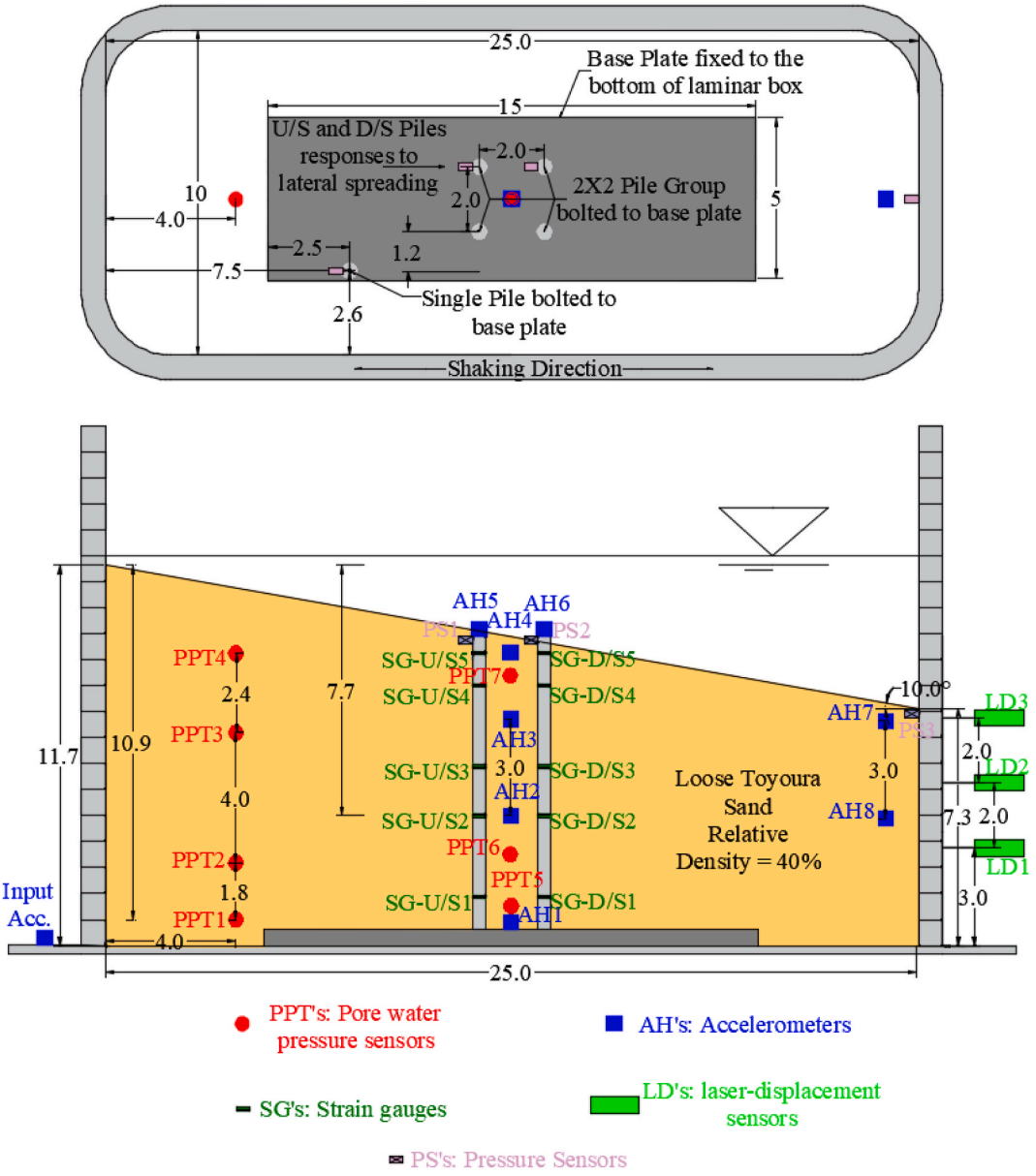

Fig. 3. Test layout for Model UL10 in top and front view (All dimensions are reported in meters in prototype scale); U/S: Upslope Pile and D/S: Downslope Pile.

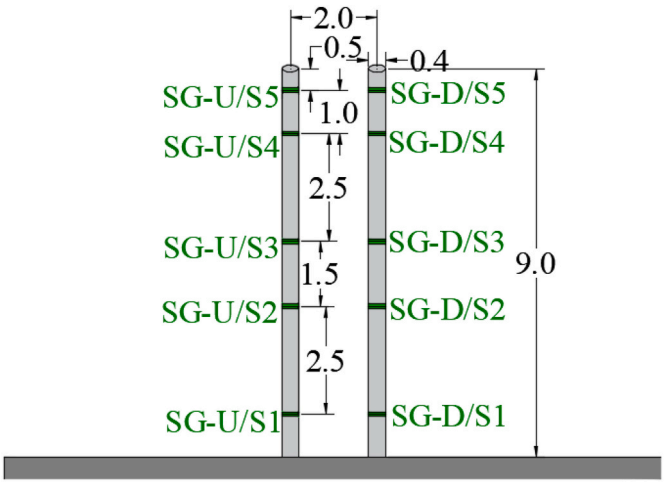

Fig. 4. Pile layout (All dimensions are reported in meters in prototype scale).

Table 1
Physical Properties of aluminium pile.

Property	In Model Scale	In prototype Scale
Diameter	8 mm	0.4 m
Length	180 mm	9 m
Young's Modulus	70 GPa	70 GPa
Second Moment of Area, I	201.06 mm^4	$1.25X10^{-3}$ m^4

subjected to nearly similar intensity of shaking for the four different events, and an effective comparison could be made. The predominant excitation frequency of the four input motions and the fixed-base natural frequency of pile were same as 1Hz, in order to maximize the pile response to lateral spreading. Apart from this, detailed earthquake characteristics are shown in Table 2 (a & b).

The sequential shaking events may likely induce a change in soil properties, including densification due to post-shaking consolidation (Brandenberg et al. [33]) as well as changes in the sloping inclinations of the ground surface; eventually turning a slope into a plain ground. With

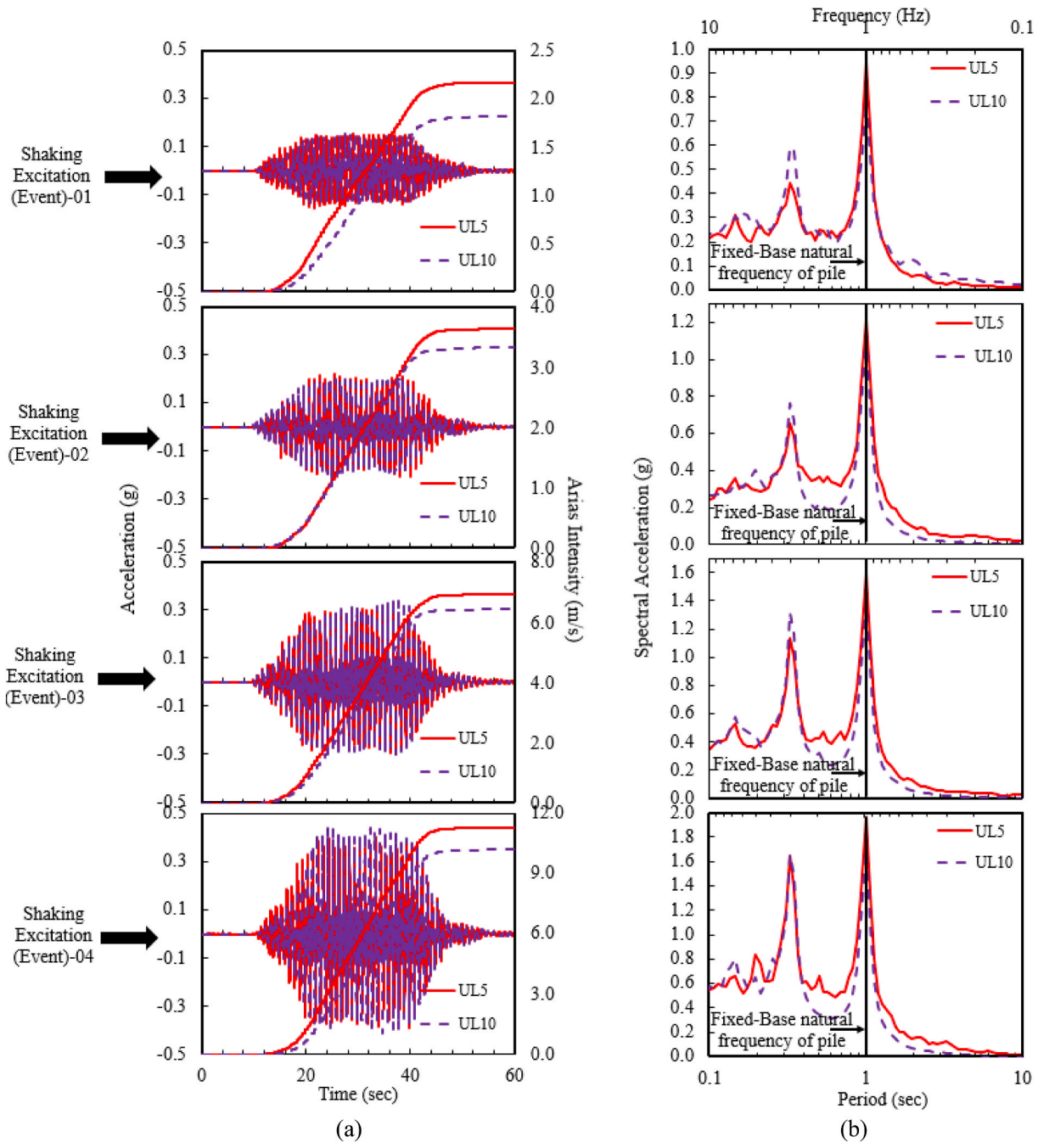

Fig. 5. Input motions achieved at the bottom of laminar box in centrifuge showing: (a) Acceleration time history and Arias Intensity (b) Acceleration response spectra (5% damped).

Table 2a
Earthquake characteristics of the four motions recorded at the base of laminar box for Model-UL5.

Motion	Peak ground acceleration (g)	Significant duration, $D_{5\text{-}95}$ (sec)	Arias intensity (m/sec)	Mean period (sec)	Standarized CAV (g*sec)
1 (SE1)	0.15	25.75	2.17	0.88	1.65
2 (SE2)	0.21	25.27	3.64	0.88	2.15
3 (SE3)	0.30	25	6.94	0.82	2.97
4 (SE4)	0.40	24.43	11.28	0.78	3.80

minor settlements due to prior shakings, the values of effective stress might change slightly; however, the changes could not be monitored, since the soil model was under fully submerged conditions and hence same effective stresses are considered in the analysis. Also, an in-flight CPT could not be used to track changes in soil properties as it could not be mounted over the laminar box; due to movement of laminar rings during shaking. Although, the preceding shaking event might cause an increase in liquefaction resistance of sand during the succeeding

Table 2b
Earthquake characteristics of the four motions recorded at the base of laminar box for Model-UL10.

Motion	Peak ground acceleration (g)	Significant duration, D_{5-95} (sec)	Arias intensity (m/sec)	Mean period (sec)	Standarized CAV (g*sec)
1 (SE1)	0.15	24.42	1.81	0.81	1.37
2 (SE2)	0.21	24	3.34	0.82	1.84
3 (SE3)	0.35	23	6.45	0.72	2.67
4 (SE4)	0.44	23	10.20	0.69	3.37

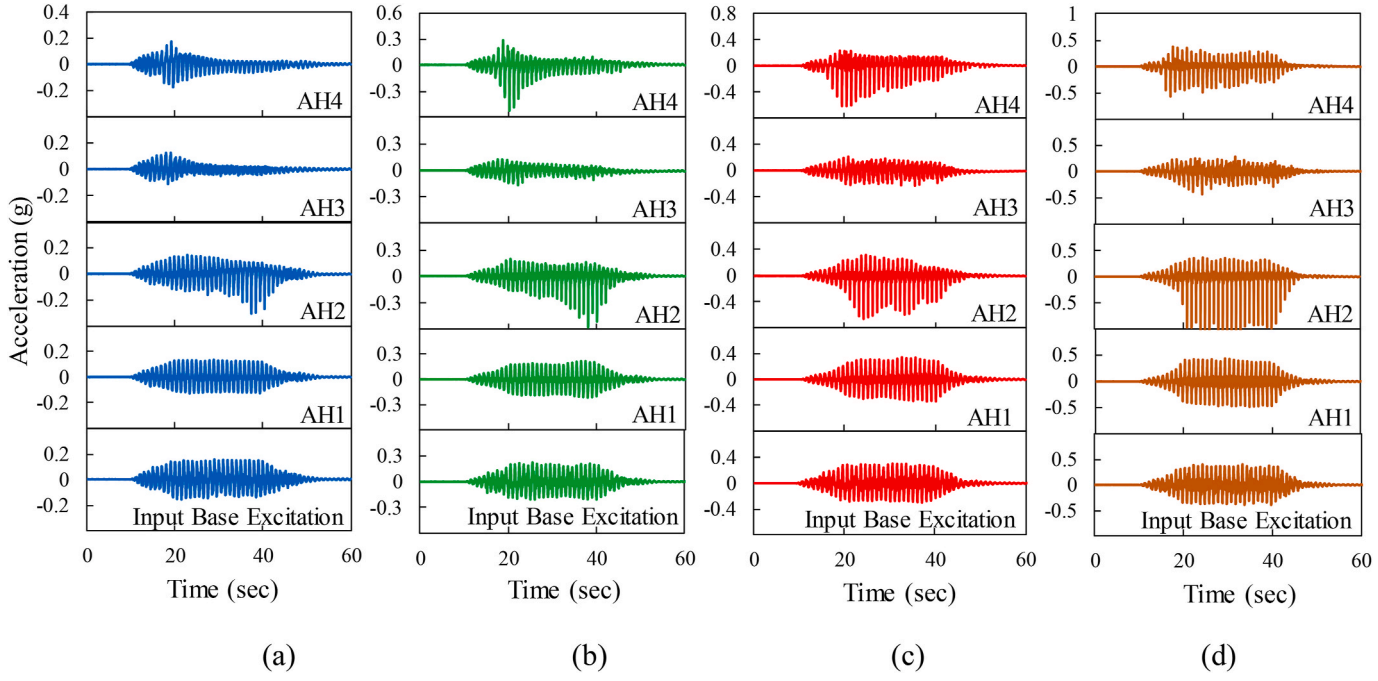

Fig. 6. Acceleration time response at the center array throughout the depth of soil model for UL5 (a) SE1 (b) SE2 (c) SE3 (d) SE4.

earthquake. Nonetheless, the succeeding earthquake event had larger intensity inducing the conditions of soil liquefaction and extensive softening near the piles, shown later in the form of excess pore pressure responses. Also, while excavating the soil model; the soil especially near the piles was found to be in a very loose state, indicating the changes in relative density would be very negligible.

3. Experimental results and observations

3.1. Acceleration response

3.1.1. Soil acceleration response for UL5

Fig. 6 shows the soil acceleration time history along the center array (near the pile foundation) for UL5. The soil at shallow depth seems to liquefy at the early stages of loading (20 s) owing to very small confining stresses. The response of soil in terms of horizontal acceleration during lateral spreading seems to be nearly similar during the first two shaking events, with spiky acceleration being observed at AH2 and AH4. These spikes become larger and unsymmetrical under the larger amplitude of base excitations (see Fig. 6(c) and (d) during SE3 and SE4) at AH2 (located near the base of soil model). The shear-induced dilative spikes are also captured near the pile head (at AH4), which shows spikes for a considerable smaller duration as compared to AH2. These unsymmetrical spikes near the ground surface are due to the flow of liquefied soil under the larger amplitude of earthquake excitation and are concentrated towards the downslope direction, with no spikes being recorded in the upslope direction. Previous researchers [1,8,9,34,35] have reported similar observations in the liquefied soil responses having dilatancy spikes. It is also explained later with the help of E.P.W.P near the pile head which shows a decreasing response preceded by an initial increase during the shaking phase owing to the shear-induced dilative behavior manifested by the liquefied soil near the pile head during SE1. Hence, this portray the presence of dilative tendency of soil in the center array of the model near the piles and this process of subsequent hardening and softening may represent a complex loading scenario on the piles.

3.1.2. Soil acceleration response for UL10

Fig. 7 shows the soil acceleration time history along the center array (near the pile foundation) for UL10. Data is not shown for the AH4 sensor, which malfunctioned during the test. A significant reduction in the amplitude of acceleration (de-amplifications) can be observed for UL10 owing to a significant amount of softening as compared to UL5. The larger negative spikes in the acceleration data towards the downslope direction, which were captured for UL5 at AH2, is found to be absent for UL10. The amplitude of acceleration remaining at a low level throughout the shaking phases for UL10 resembles soil having very low residual shear strength throughout the depth (particularly at AH2 near the base of soil model). This softening response is also explained later in section 4 with the help of excess pore pressure response, which builds up in a short time compared to UL5 for all the shaking events. The increase in the shaking intensity is found to have a minor influence on the acceleration response, with the response remaining nearly identical during all the shaking events, with the soil remaining relatively soft exhibiting different behavior to what was observed for UL5. Fig. 8 shows the soil acceleration responses near the downslope side (free-field). From the Fig., one can observe that the reduction in amplitude is not significant towards the ground surface during SE1, which may indicate

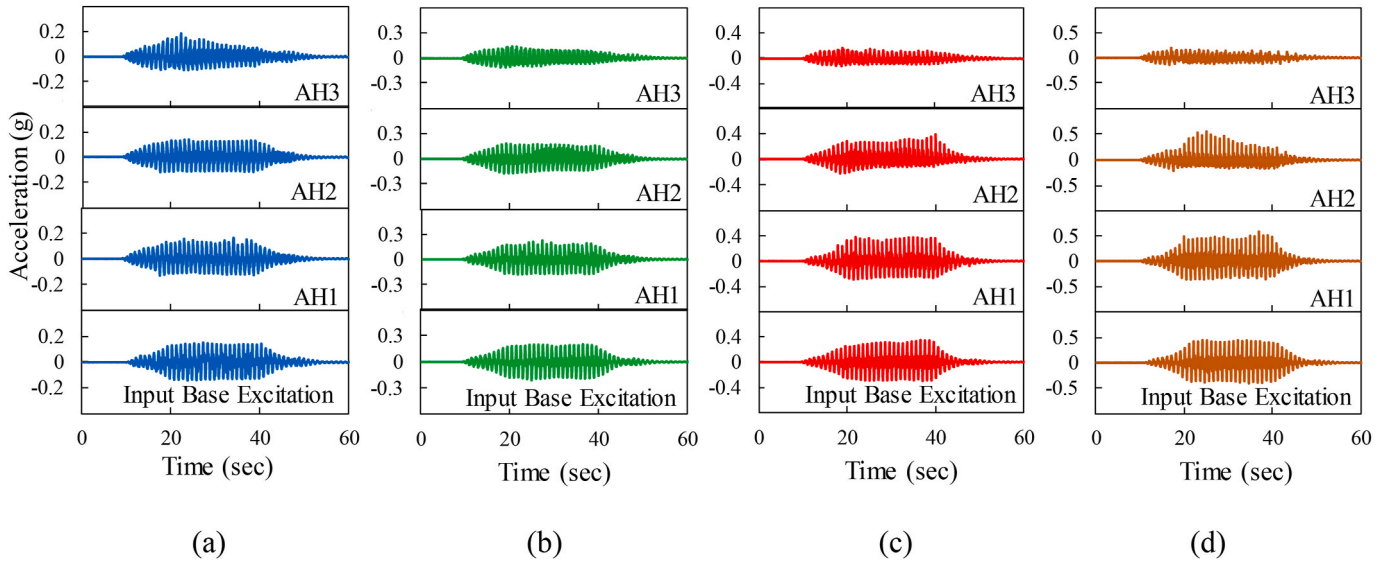

Fig. 7. Acceleration time response at the center array throughout the depth of soil model for UL10 (a) SE1 (b) SE2 (c) SE3 (d) SE4.

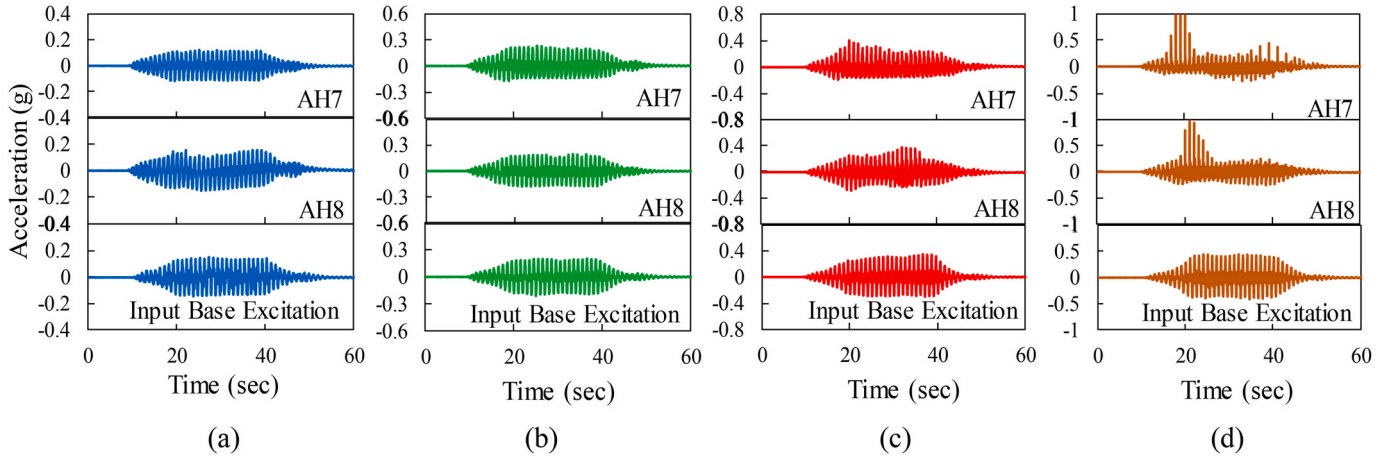

Fig. 8. Acceleration time response at the free field (downslope side) throughout the depth of soil model for UL10 (a) SE1 (b) SE2 (c) SE3 (d) SE4.

comparatively smaller magnitude of flow of liquefied soils near the downslope side. However, with the increase in intensity of earthquake, significant de-amplifications with larger spikes could be observed towards the ground surface during the shaking.

3.2. Excess pore pressure response

3.2.1. Excess pore pressure for UL5

Fig. 9 shows the free field excess pore pressure response for UL5 with the incremental shaking intensities. The condition of soil liquefaction defined as EPWP ($r_u=u_e/\sigma_{vo}'$) = 1.0 was achieved quickly near the ground surface (shown by horizontal line for all the cases), where u_e is the excess pore pressure generated under earthquake loading and σ_{vo}' is the initial effective vertical stress. The excess pore pressure response indicates the beginning of dissipation from the bottom layer, followed by the upper layer in the soil model. Importantly, excess pore pressure having positive and negative amplitude was found to develop near the ground surface at PPT4 during SE2 as shown in Fig. 9(b). One of the important observations is the initiation of the attainment of soil liquefaction, which occurs more rapidly with few loading cycles with the increase of the shaking intensity (see PPT1 and PPT2, located towards the bottom of soil model); interestingly, the dissipation starts lately for the higher magnitude of base excitations. This response shows soil experiencing greater softening while remaining for a longer time at the liquefaction phase before ultimately showing a hardening phase with the initiation of dissipation. The significant magnitude of the dynamic oscillations or shear-induced dilative spikes is found to be present for sensors located near the ground surface under lower confining stress,

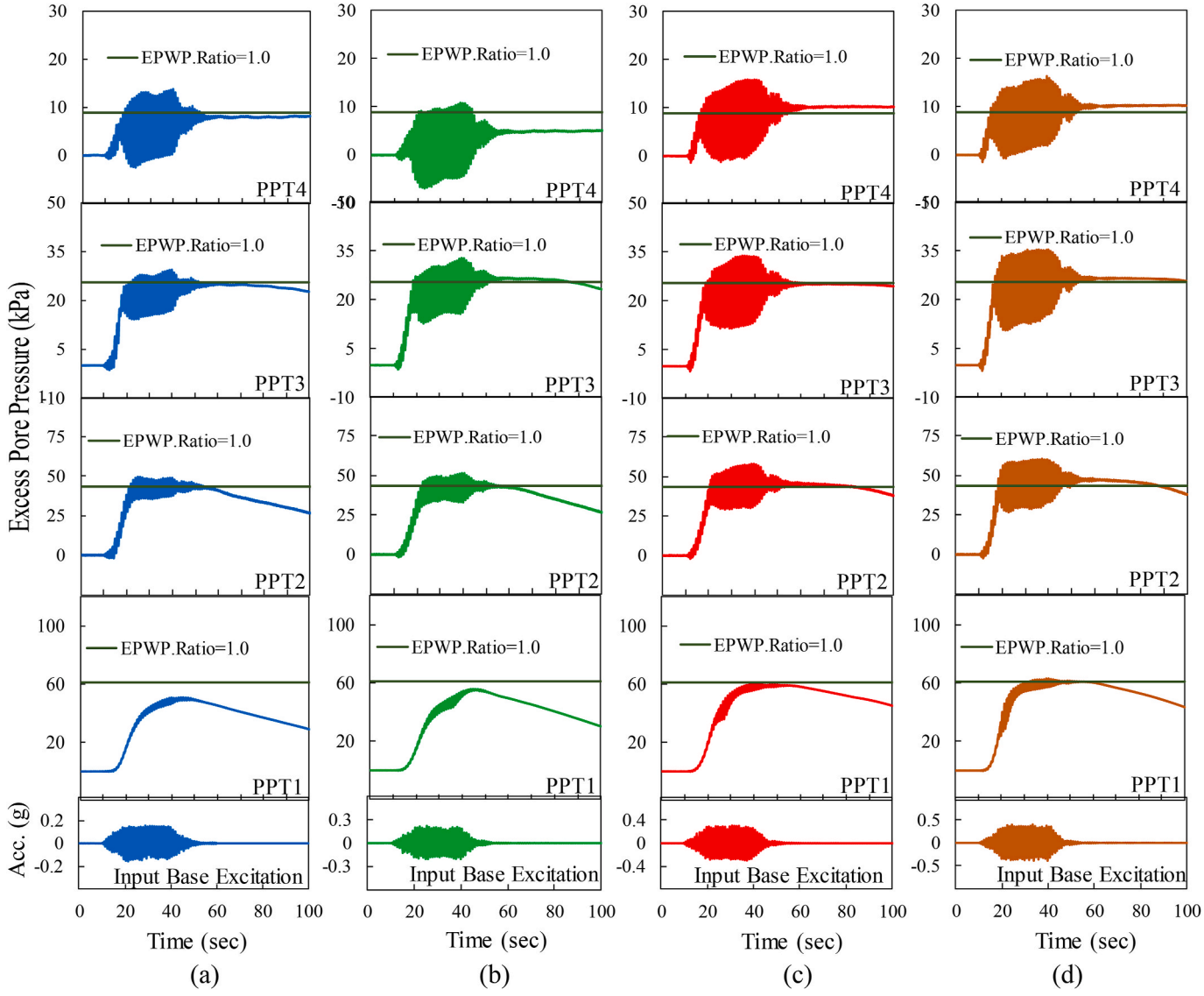

Fig. 9. Free field excess pore water pressure responses for UL5 (a) SE1 (b) SE2 (c) SE3 (d) SE4.

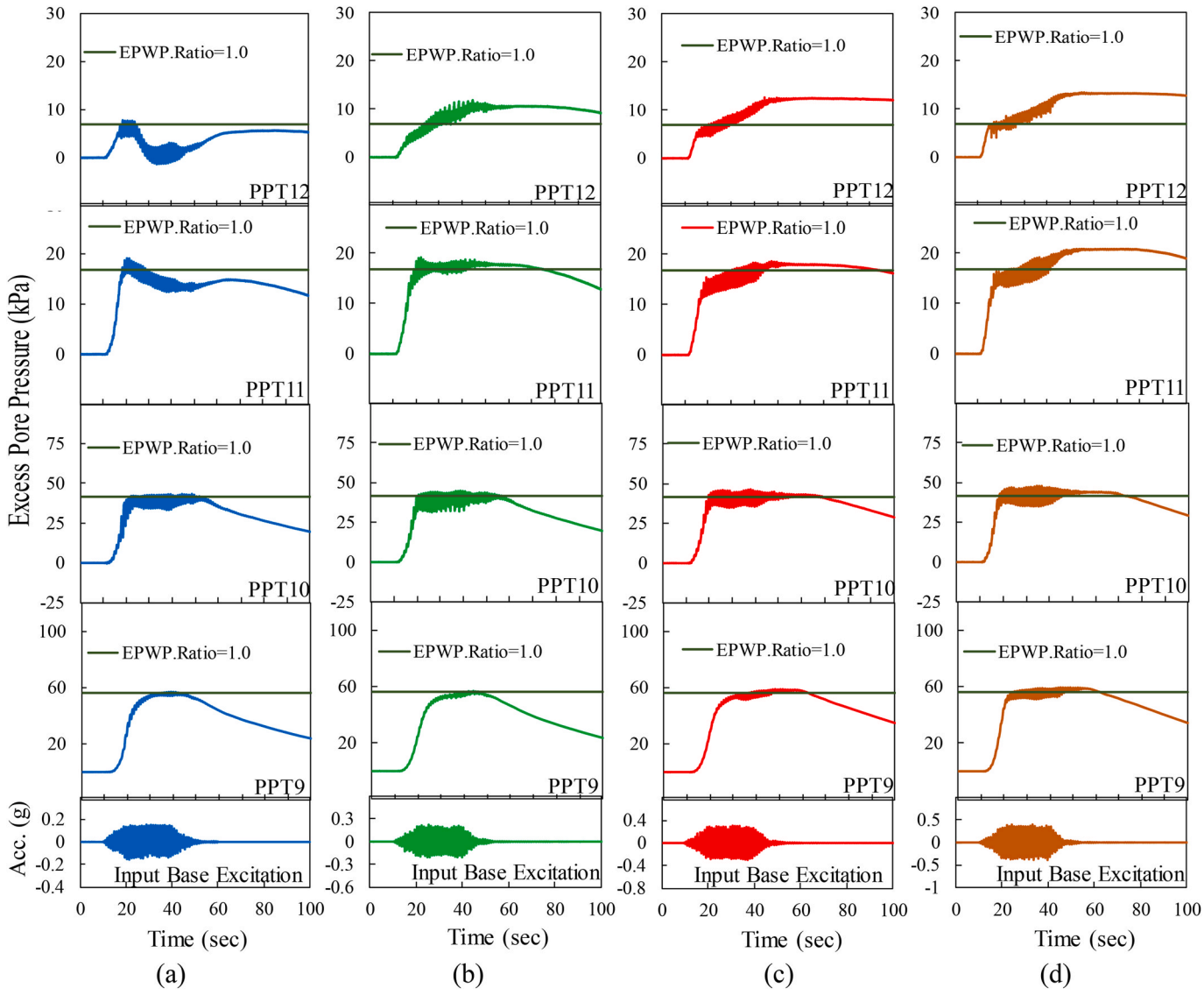

Fig. 10. Excess pore water pressure responses (near piles) for UL5 (a) SE1 (b) SE2 (c) SE3 (d) SE4.

which indicates larger magnitude of flow of liquefied soil near the ground surface.

Fig. 10 shows the excess pore pressure response near piles for UL5. One of the key observations is the occurrence of soil liquefaction throughout the depth near the piles during SE1 contrast to the free field response. The excess pore pressure response near piles posits the absence of large dynamic oscillations that were captured in the free field response. The upward gradient is relatively larger near piles than the free field with the condition of soil liquefaction achieving rather quickly. These results show soil being softer near the piles as compared to the upslope side, which represents the absence of shear-induced dilative behavior in the center array of soil model which might affect the kinematic response of a group pile.

3.2.2. *Excess pore pressure for UL10*

Fig. 11 shows the free field excess pore pressure response for UL10. The spikes are found to be more profound near the base of soil model (see PPT1, PPT2 and PPT3), with minor oscillations being observed for PPT4. This indicates, the response near the far field (upslope side) for UL10 to have a considerable shear-induced dilative response towards the bottom of soil model, as compared to larger spikes being captured for UL5 near the ground surface. With soil liquefying early during the shaking phase under a higher amplitude of base excitation, the magnitude of oscillations is also found to increase. Intriguingly, the initiation of the dissipation phase for all the shaking events is not found to depend on the magnitude of excitation and is the same for SE1 through SE4.

Fig. 12 shows the excess pore pressure response near the piles for UL10, where soil liquefaction is achieved throughout the center array during all the shaking events. Unfortunately, PPT6 did not work and hence the results are not shown for PPT6. The differences in the dilative oscillations near the bottom of soil model (between upslope and center array) for UL10 was considerably larger than what was observed for UL5 (shown in Figs. 9 and 10). These results indicate the soil in the center array of the model to be significantly softer than the upslope side. It can be corroborated by the E.P.W.P. ratio values, near the bottom of soil model (PPT5) which are of higher magnitude as compared to the E.P.W.

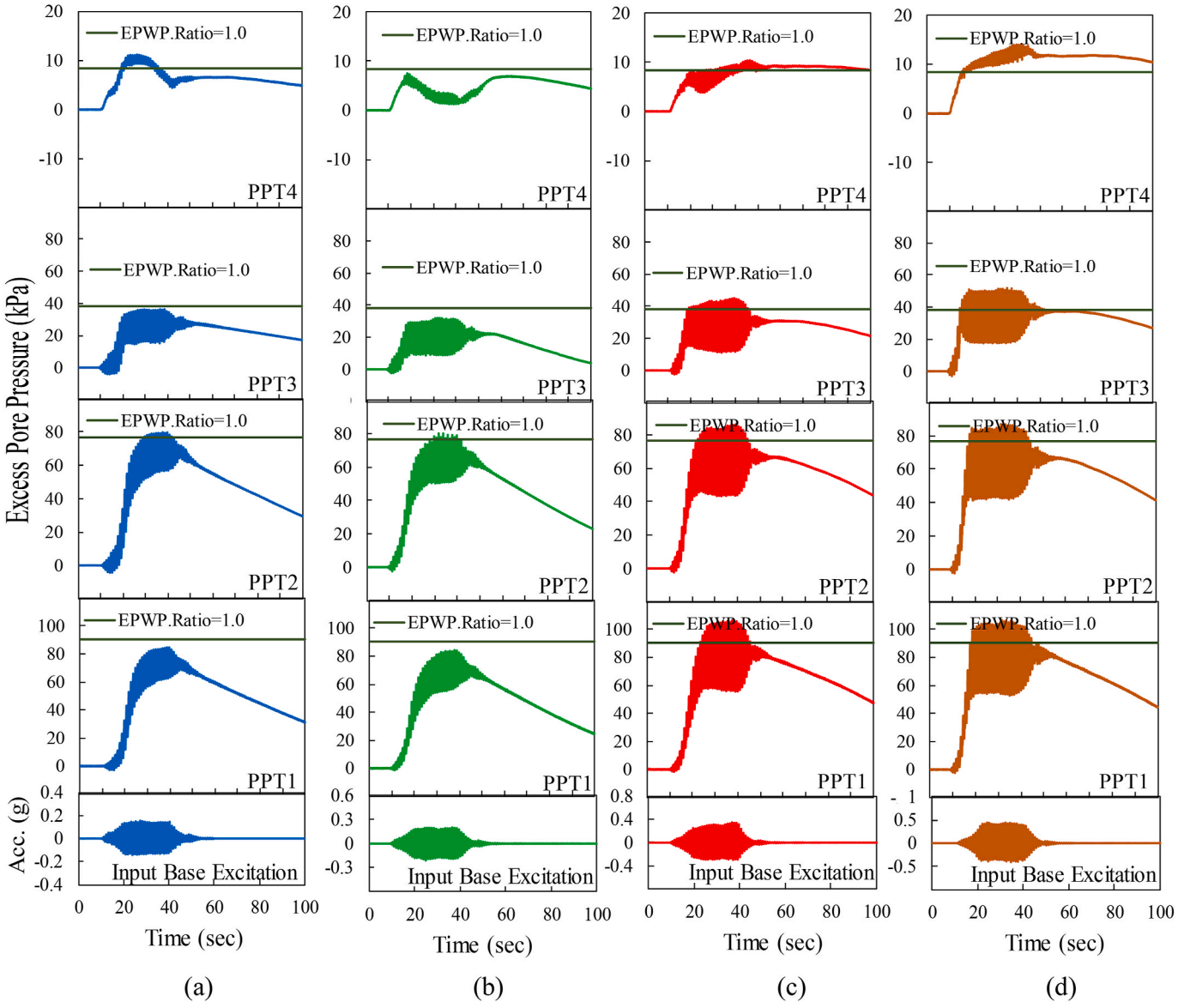

Fig. 11. Free field excess pore water pressure responses for UL10 (a) SE1 (b) SE2 (c) SE3 (d) SE4.

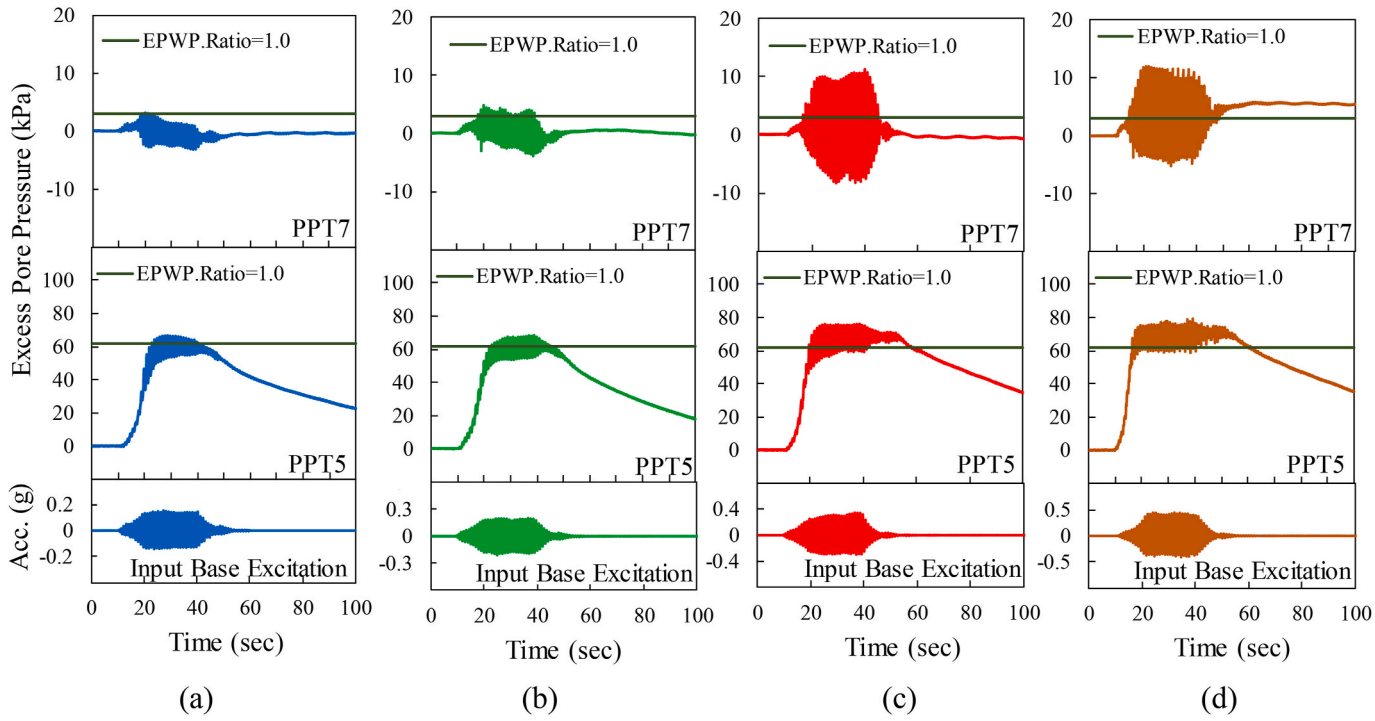

Fig. 12. Excess pore water pressure responses (near piles) for UL10 (a) SE1 (b) SE2 (c) SE3 (d) SE4.

P. ratio values obtained for UL5 during all the SEs (shown in Fig. 10). Similar to the E.P.W.P. response near the ground surface at the upslope side, the E.P.W.P. near the pile head in the center array shows an initial increase followed by the decreasing response developing significant negative amplitude. It is also worth mentioning that the flow of liquefied soil around the pile head may be larger under higher intensity earthquakes as shown in Fig. 12 for PPT7 with the increasing oscillations being obtained.

Some of the researchers in past (e.g. Gonzalez et al. [36], Chaloulos et al. [37,38]) have shown the development of negative excess pore pressure near the pile head (declining from the onset of shaking) using centrifuge and numerical modeling. In the present study, an initial rise in the E.P.W.P. leading to the occurrence of soil liquefaction is observed during the first shaking and to the occurrence of largest kinematic bending moments (explained later in section 5). However, soon after the liquefaction, with the liquefied soil flowing, a decreasing E.P.W.P response is obtained both near the pile head and the upslope ground surface. Substantially higher negative values were obtained for UL10 as compared to UL5, which also increased with the increase in shaking intensity. This indicates the flow of liquefied soil around the pile head towards the center array may be larger for UL10 as compared to UL5.

3.3. Lateral soil displacement responses

Fig. 13 shows the lateral soil displacement time history responses measured at the ground surface near the downslope side recorded using the laser displacement sensor. Larger magnitude of lateral displacement is induced near the ground surface for UL10 as compared to UL5 during all the shaking excitations. The typical soil lateral displacement response is very similar to the kinematic moment responses showcased by the pile during an earthquake; shown later in section 4, which indicates the pile to follow the soil movement. Although the cyclic soil displacement increases in magnitude (see UL5 response during SE4); extensive softening and the flow of liquefied soil imparts little kinematic moments onto the pile surface during higher intensity earthquakes; discussed in section 4 and 5. It may be evident from Fig. 13, that predominant lateral spreading takes place during the first excitation, having unidirectional drift; perhaps displacement recording larger cyclic components with the increase in shaking excitations, indicating the sloping configuration of a soil model turning into a plain model configuration.

In order to assess the influences of soil displacements on the soil-pile kinematic interactions during lateral spreading, where permanent monotonic soil displacements are a bigger concern; cyclic components from the displacement responses were removed using an averaging filtering procedure. Fig. 14 presents the maximum lateral soil displacement (monotonic responses) along the depth and the results are plotted at different time instances during an earthquake loading. Although the soil achieves a state of liquefaction, around 20–30 s at most of the locations in a soil model (see excess pore pressure responses); the lateral soil displacement continues to rise till 40 s; however, showing the similar responses from 40 to 60 s (see Fig. 14(a) during SE1). This is the time instance, when the generated excess pore pressure starts dissipating; commencing the process of regain in shear strength of soil; explained in a detailed way in section 4 (see Fig. 19(a) during SE1). The magnitude of maximum lateral soil displacement is found to decrease during SE2, which indicates lesser monotonic soil displacements being imparted onto the piles, which reduces the kinematic moment demands in piles as shown in section 4.

Fig. 15 shows the maximum monotonic lateral soil displacements along the depth (a) during SE1 and (b) during SE2 for UL10 soil model. Under a larger sloping inclination, notably larger lateral displacements are recorded as compared to a mild and smaller inclined ground model i. e. UL5. The larger monotonic displacements would have huge significance on the soil-pile kinematic interactions. The soil records maximum displacements just before the end of shaking and shows similar responses till 60 s as shown in Fig. 15 (a) and 15(b). This indicates the predominant flow of liquefied soils to continue even after the end of shaking representing importance of post-shaking lateral displacements. With the increase in shaking intensity, the lateral displacement is found to reduce, which indicates predominant lateral spreading to take place during the first excitation.

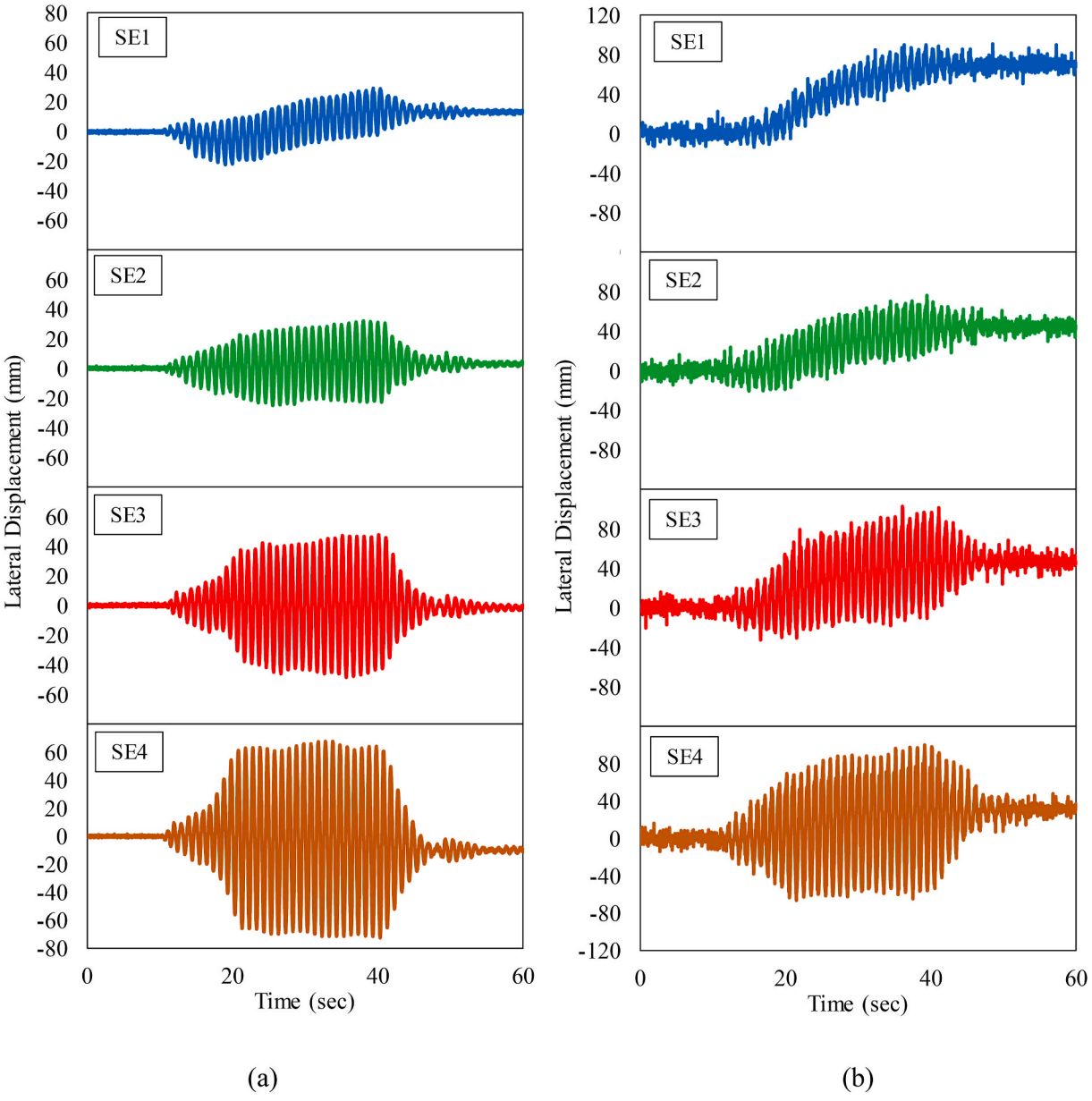

Fig. 13. Lateral soil displacement (a) UL5 maximum response measured at ground surface (b) UL10 maximum response measured at ground surface.

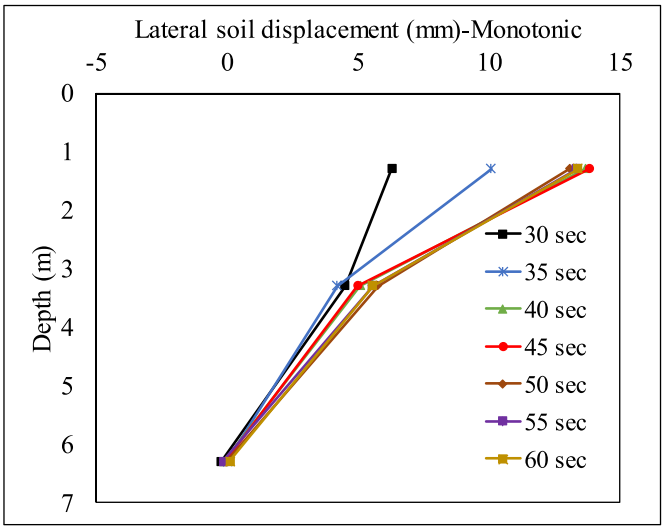

(a)

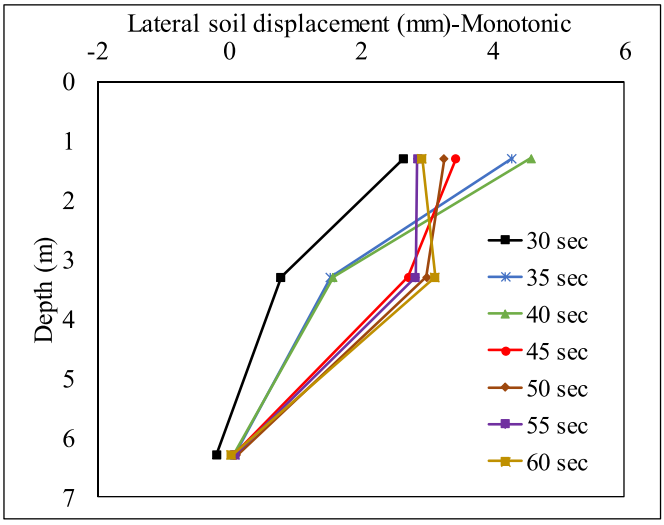

(b)

Fig. 14. Lateral soil displacement for UL5 (Monotonic responses) (a) SE1 (b) SE2.

3.4. Velocity time-history responses

In order to assess the rate-dependency nature of liquefied soils, the measured acceleration responses are converted to velocity time-history along the center array. With the occurrence of liquefaction and the flow of liquefied soils, higher velocity rate is measured during the shaking as shown in Fig. 16. The magnitude of flow rate of liquefied soil is largest towards the ground surface. The rate is found to increase with the increase in shaking intensity; similar to what was captured in the lateral soil displacement responses. Unfortunately, the velocity responses are not shown near the ground surface for UL10 due to the malfunctioning of accelerometer. However, larger velocity flow rate is estimated at the mid-depth of soil model for UL10, which may indicate the differences in the flow rate of liquefiable soils based on the sloping inclinations of the ground surface.

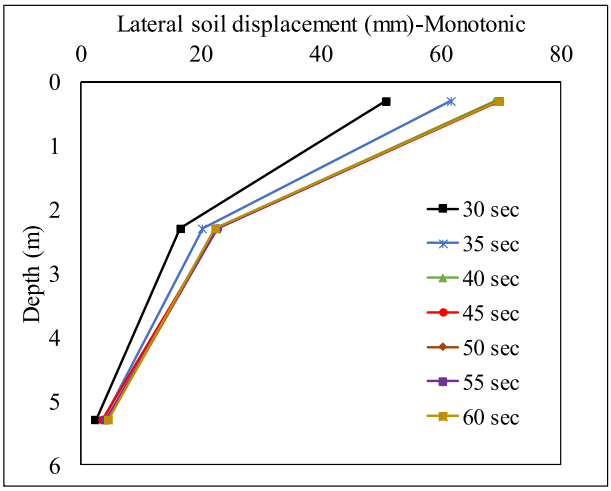

(a)

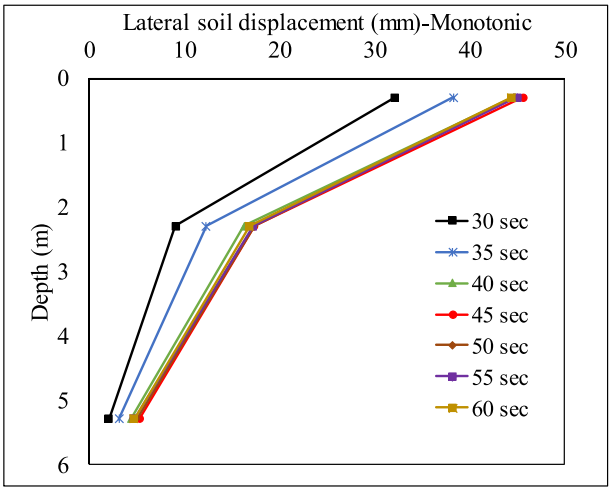

(b)

Fig. 15. Lateral soil displacement for UL10 (Monotonic responses) (a) SE1 (b) SE2.

3.5. Lateral earth pressure acting on the piles during lateral spreading

Earth pressure sensors were installed along the length of UL10-Model and were placed on the upslope pile, downslope pile and at the downslope side near the ground surface towards the direction of lateral spreading. The earth pressure sensor placed at the downslope pile malfunctioned during the test and hence the results are omitted. The lateral soil pressure is found to increase towards the water-side or downslope side, with the larger magnitude of flow of liquefied soil taking place near the downslope side as shown in Fig. 17. The findings are well in consent with available literature [20,22], indicating the larger soil pressure or moments to act towards the pile located near the waterside resulting in the tilting of the superstructure towards waterside.

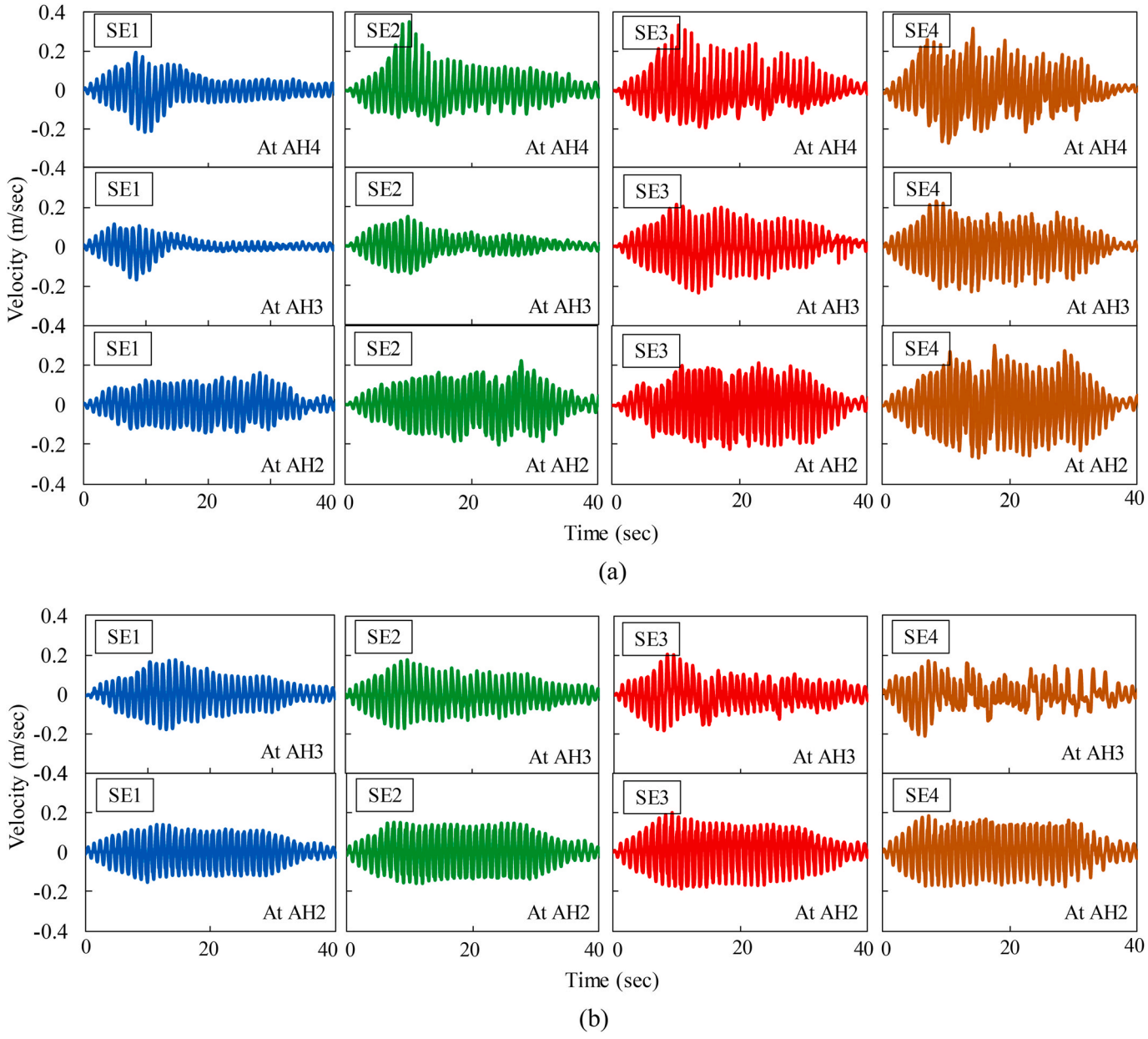

Fig. 16. Velocity time history responses along the center array (a) UL (b) UL10.

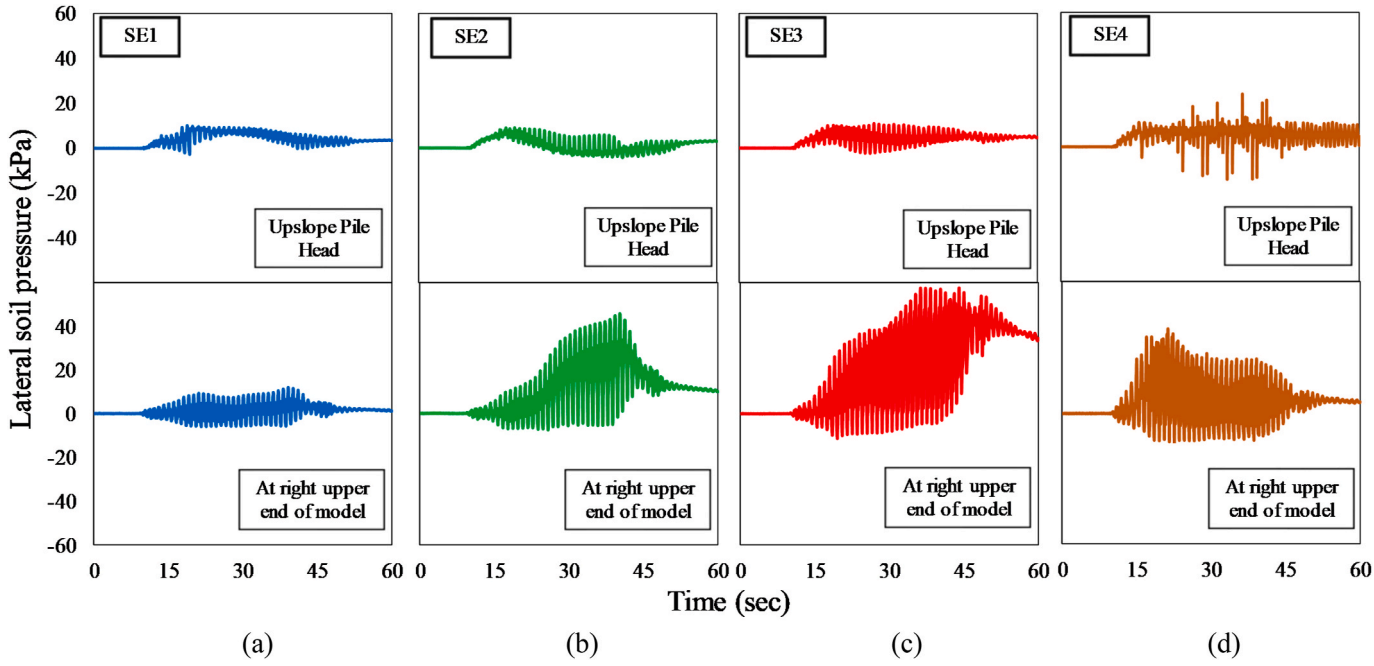

Fig. 17. Lateral soil pressure responses during different shaking excitations for UL10.

3.6. Fourier amplitude responses at the pile head

Accelerometers were placed on the upslope and downslope pile head to assess the soil-pile kinematic interactions depending on different sloping inclination angles of the ground surface and under different intensity of earthquakes. Fig. 18 shows the smoothed Fourier amplitude plotted versus period measured at the pile head for different cases. The data could not be collected properly for the upslope pile during SE3 for UL5 and hence is not shown in Fig. 18(a). The maximum response at the pile head was evaluated at a frequency of 1 Hz, which is the fixed-base natural frequency of piles during all the shakings as shown in Fig. 18. One can observe the downslope pile recording larger Fourier amplitude for both the cases i.e. UL5 and UL10, which highlights the similar trend shown later in section 4 and 5, with the downslope piles recording larger kinematic moments. Slightly larger responses captured for both the upslope and downslope piles for UL10 model may be due to the larger amount of flow of liquefied soil around the pile head as compared to UL5 as shown initially from the E.P.W.P. response near the pile head (shown in Figs. 10 and 12). In the case of UL10, similar magnitude of Fourier amplitude was measured at the upslope pile head; however, the responses were observed to increase with the increase in shaking amplitude for the downslope pile. This may indicate the soil-pile kinematic interactions during a lateral spreading phenomenon to depend significantly on the location of pile within a group.

4. Influence of excess pore pressure generation on the maximum kinematic bending response of upslope and downslope pile

The kinematic bending response which is predominant near the lower section of piles depend on the state of soil around the bottom section of pile. This may represent a complex interaction with the surrounding soil experiencing soil liquefaction exhibiting the presence of strong non-linearity near the bottom section of pile. Previous researchers e.g. Ebeido et al. [24] found the maximum moment for the upslope and downslope pile to occur around the onset of liquefaction. However, the piles were connected to a pile cap which may impart the inertial loading as well and hence the response cannot be considered purely due to the kinematic interactions. A study carried out by Motamed et al. [20] to investigate the soil-pile kinematic interactions indicated the maximum lateral forces and bending moment experienced by the front piles during lateral spreading to occur around the onset of liquefaction. Apart from these, no to very few studies have been carried out to the best of authors knowledge to examine the influences of the generation and dissipation process of the excess pore pressure on the upslope and downslope pile during lateral spreading involving kinematic interactions. Hence, in this paper, the authors examined the kinematic bending response of the upslope and downslope pile, which is maximum near the bottom of piles (measured from strain gauge SG1) with respect to the excess pore pressure measured (PPT9 for UL5 and PPT5 for UL10), which is located close to SG1 subjected to successive base excitations.

The pile surface was heavily instrumented with strain gauges on both the sides (i.e., upslope and downslope) to record the kinematic bending response of pile under the increasing amplitude of base excitation motions in both the experiments. The pile response subjected to four SEs is independently measured for a corresponding shaking by initializing all the strain gauge values to zero prior to the next SE. The bending moment was calculated from strain gauges (ε_1 and ε_2) located in the longitudinal direction at a particular depth as per equation (1) for five locations along the length of pile as shown in Fig. 4.

$$M = EI\varphi = EI(\varepsilon_1 - \varepsilon_2)/2y \quad (1)$$

Where EI is the bending stiffness of the pile, φ is the curvature of the pile, and y is the distance of the strain gauges to the neutral axis.

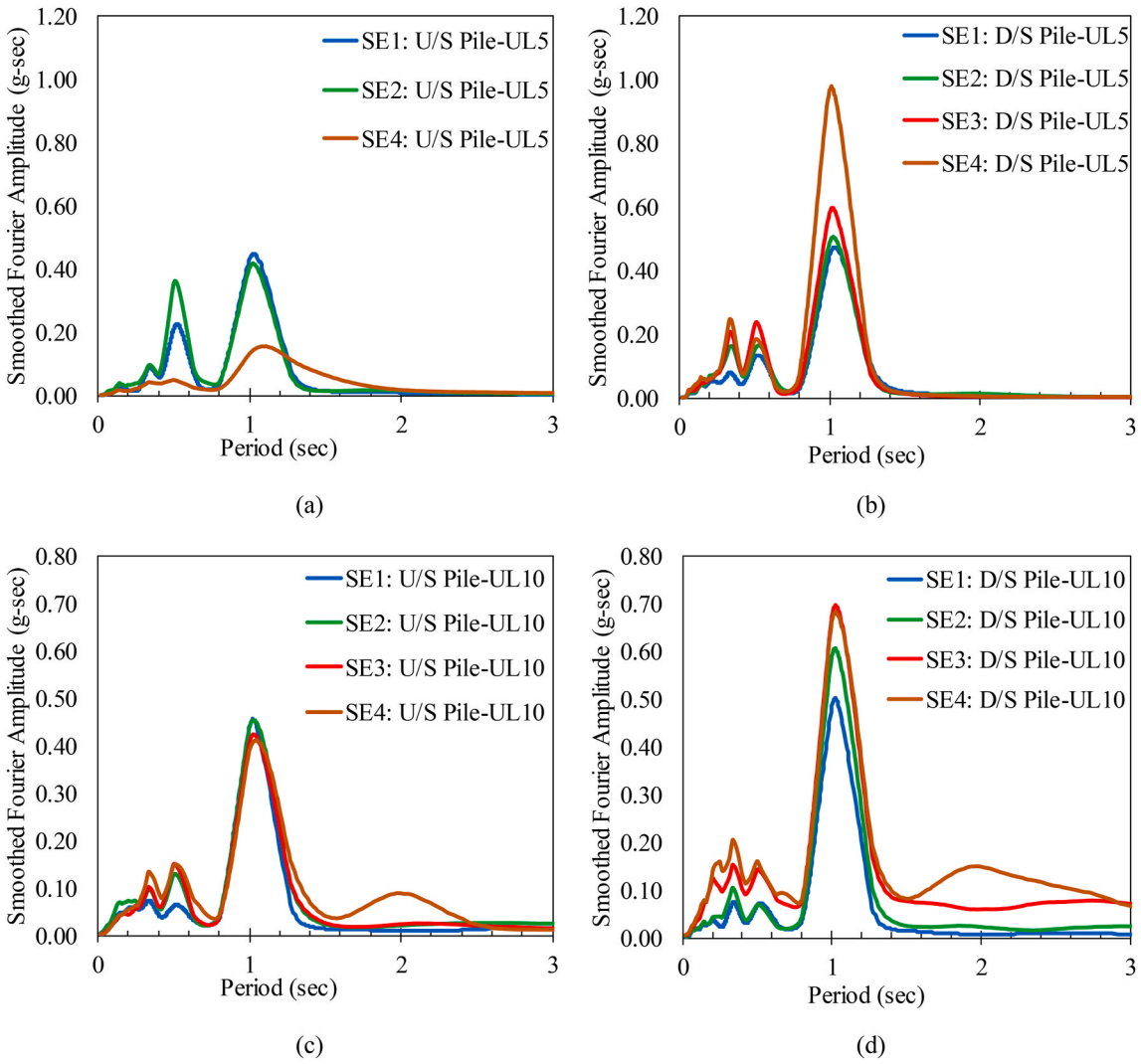

Fig. 18. Smoothed Fourier Amplitude evaluated at the pile head (a) UL5-Uplsope Pile (b) UL5-Downslope Pile (c) UL10-Uplsope Pile (d) UL10-Downslope Pile.

Fig. 19 shows the measured excess pore pressure (E.P.W.P) ratio time history from PPT9 and the kinematic bending moment time history for the upslope and downslope pile during the four successive earthquake loadings for UL5. From Fig. 19(a), during SE1, the upslope pile recorded maximum moment at 27.8 s, just before the initiation of soil liquefaction at 34 s. However, the downslope pile recoded maximum moment at a time instance of 40 s, just before the initiation of the dissipation of excess pore pressure. Hence, it can be said that the upslope and downslope pile may receive maximum kinematic moments at different time during an earthquake, although the magnitude of moment for both the upslope and downslope pile was found to be considerable around the initiation of dissipation phase of excess pore pressure. During SE2, SE3, and SE4 which involves higher magnitude of base excitation, both the upslope and downslope pile received maximum kinematic moment before the occurrence of soil liquefaction as shown in Fig. 19(b), (c) and 19(d). However, considerable moments were generated till 40 s before the beginning of dissipation phase of excess pore pressure. Just few secs before the initiation of dissipation phase, the moments start reducing significantly and records residual value close to zero (see Fig. 19(c) and (d) for SE3 and SE4). Soil remaining in a state of liquefaction for a larger duration under a higher magnitude earthquake during SE3 and SE4 may be responsible for the drastic reduction in the moment values. Apart from this, initial sloping ground model turning into a plain ground; with now the lateral loading acting in both the directions, may also be the reason for such a decrease in moment demands even under higher earthquake excitation as compared to the case of predominant lateral spreading during SE1.

Fig. 20 shows the E.P.W.P. ratio and the maximum kinematic moment response during the different shaking events for UL10. One of the important observations is the upslope and downslope pile receiving maximum moment at the same time during all the shaking events. The maximum moment recorded by the upslope and downslope piles during SE1 and SE2 is around the initiation of dissipation phase of excess pore pressure. The kinematic moment increases progressively (for upslope and downslope pile) during SE1 up till achieving the largest values followed by the reduction soon after the initiation of dissipation phase. This is in contrast with UL5, where significant moment was already developed before the occurrence of soil liquefaction (for upslope and

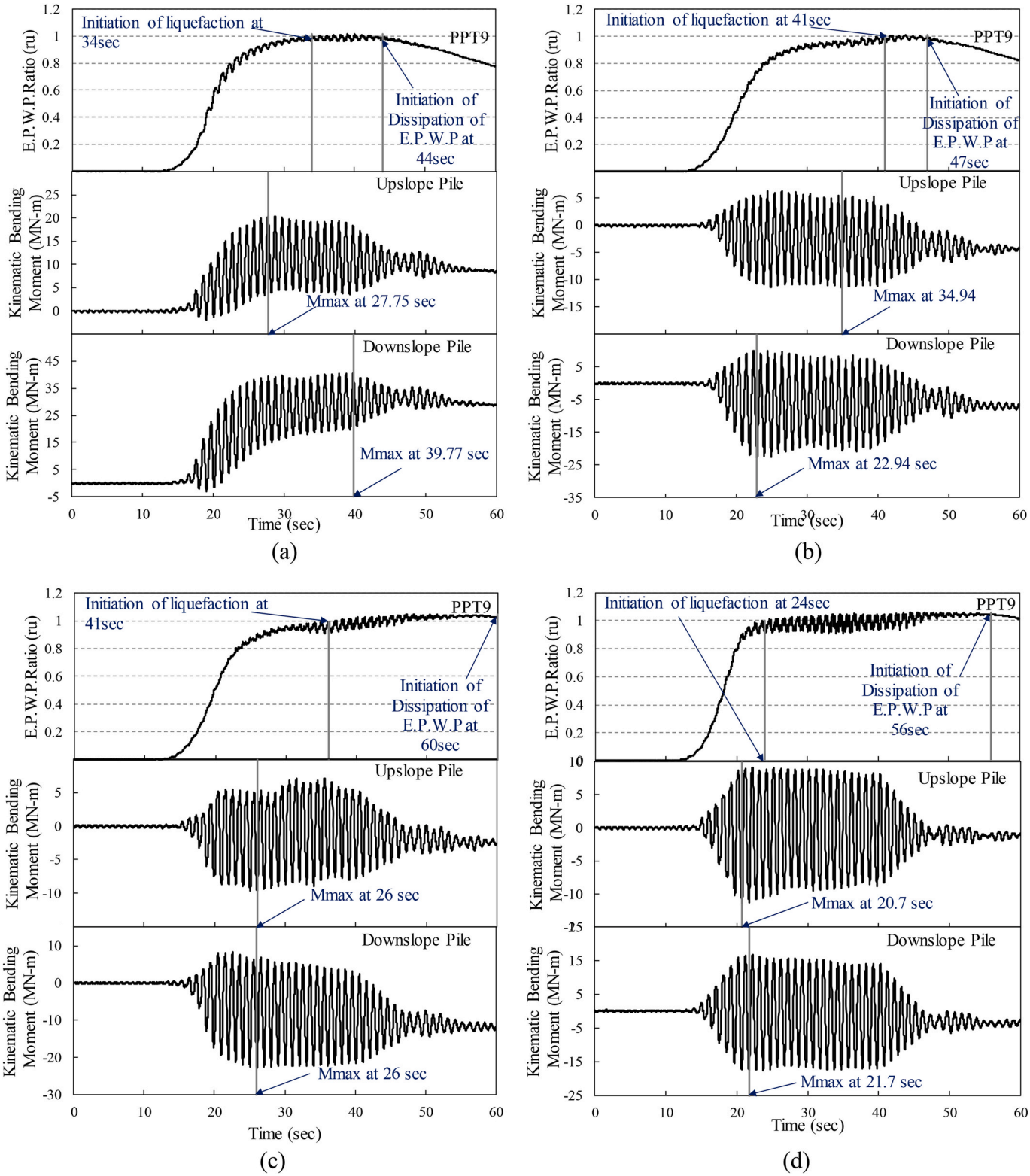

Fig. 19. Influence of the excess pore pressure generation on the upslope and downslope pile for UL5 (a) SE1 (b) SE2 (c) SE3 (d) SE4.

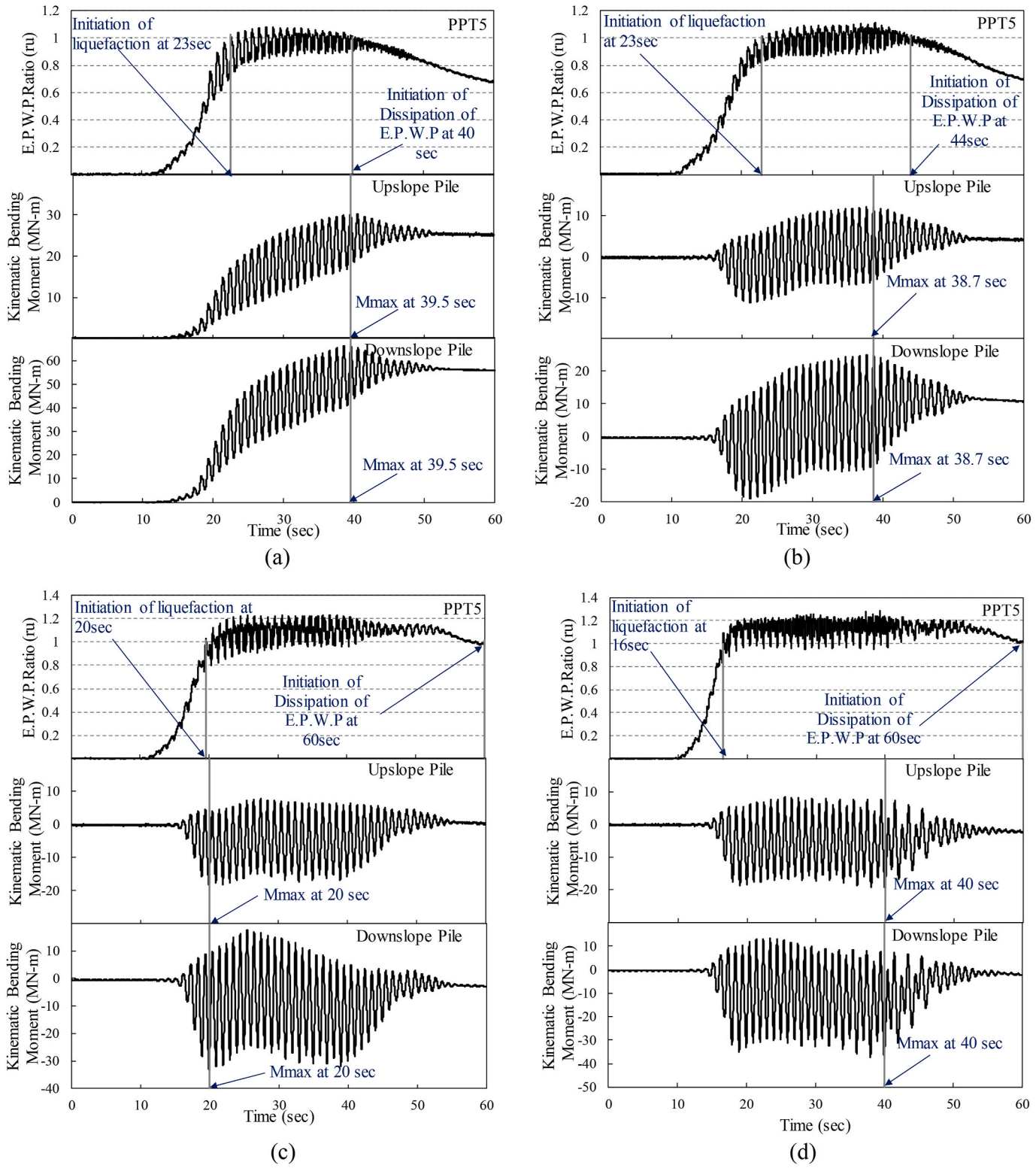

Fig. 20. Influence of the excess pore pressure generation on the upslope and downslope pile for UL10 (a) SE1 (b) SE2 (c) SE3 (d) SE4.

downslope pile). During SE3 and SE4 as shown in Fig. 20(c) and (d), the piles showed considerable moment demands till around 40 s following with the significant reduction in the values with nearly zero moment measured as a residual value. This is because of the soil remaining in a state of liquefaction for a prolonged time during SE3 and SE4 as compared to SE1 and SE2.

5. Kinematic bending response of the piles

In the following section, kinematic moments measured along the length of pile are discussed and compared for UL5 and UL10.

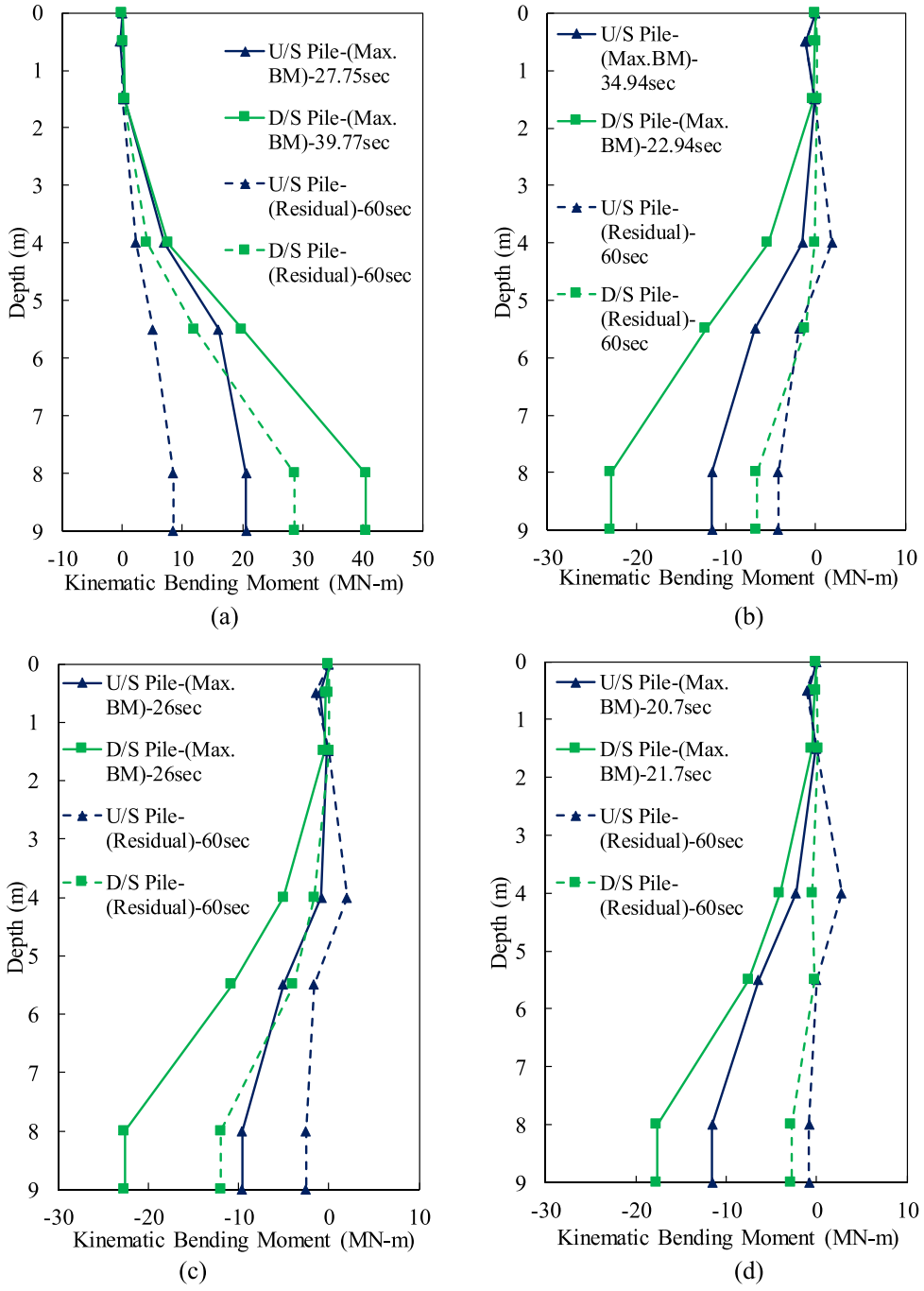

Fig. 21. Kinematic Bending Moment response of a 2X2 pile group for UL5 (a) SE1 (b) SE2 (c) SE3 (d) SE4.

5.1. Kinematic bending response of upslope and downslope piles for UL5

Fig. 21 shows the kinematic bending moment response for a 2X2 end bearing group pile (upslope and downslope) during the four SEs for the UL5 model, where U/S represents the upslope pile and D/S represents the downslope pile. As expected for a cantilever beam configuration, the maximum kinematic bending moment was found to occur near the base for both the upslope and downslope pile during all the shaking events. During the SE1 shown in Fig. 21(a), the upslope pile recorded a maximum kinematic moment of 20.58 MN-m, while the downslope pile recorded a maximum value of 40.55 MN-m, which was 1.97 times higher. Although the downslope pile still shows higher moment demands as compared to the upslope pile throughout the shaking phase for SE2, SE3, and SE4 shown in Fig. 21(b), (c) and 21(d) respectively, the magnitude of the moment is found to be reduced, with the upslope pile recording maximum values of 11.6, 9.7, and 11.5 MN-m for SE1, SE2, and SE3, respectively, while the maximum moment demands exhibited by the downslope pile during SE2, SE3, and SE4 are 22.9, 22.67, and 17.64 MN-m, respectively. With the increase in the amplitude of the base excitation, the state of soil liquefaction throughout the depth of soil model develops a bit earlier during the earthquake loading, which prompts the upslope and downslope piles to develop maximum moment demand much earlier with the increasing intensity. Soils remaining in a state of liquefaction for a significantly larger duration during the shaking phase (as discussed in section 4) near the piles throughout the depth of the model; with the lateral soil pressure acting in both the directions may also be responsible for the reduction observed in the moment demands of the piles, with the residual kinematic moments also

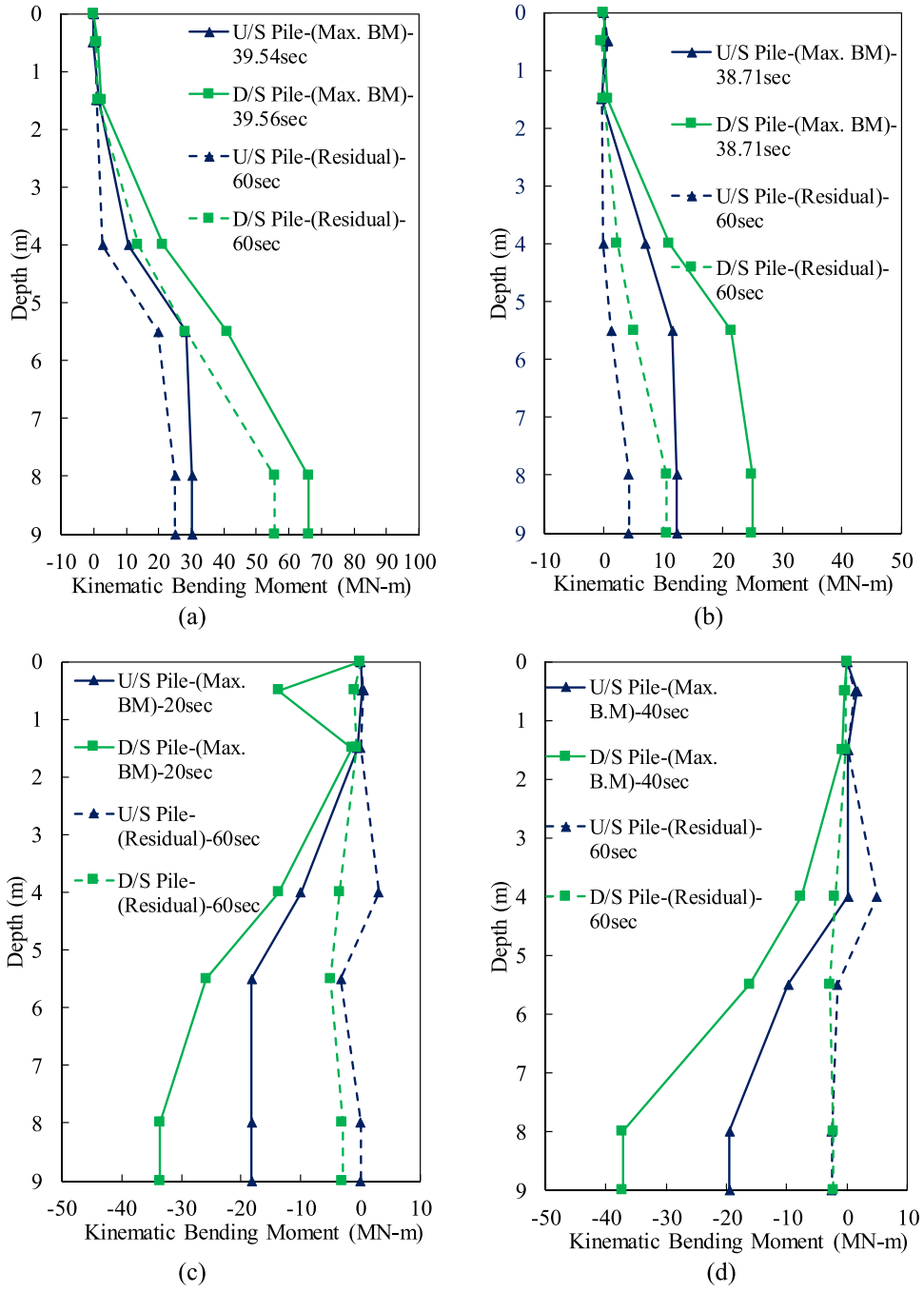

Fig. 22. Kinematic Bending Moment response of a 2X2 pile group for UL10 (a) SE1 (b) SE2 (c) SE3 (d) SE4.

showcasing drastic reduction in the values with the increasing intensity of the base excitation.

5.2. *Kinematic bending response of upslope and downslope piles for UL10*

Fig. 22 shows the kinematic bending moment response for UL10 under the four SEs. Similar to UL5, the downslope pile was subjected to significantly larger moment values compared to the upslope pile. The maximum moment in the downslope pile for UL10 is measured to be 66.21 MN-m, which is 2.18 times higher than that measured for the upslope pile (30.30 MN-m) during SE1 shown in Fig. 22(a). However, there is a sharp decrease in the maximum kinematic moment during SE2 (Fig. 22(b)), with the upslope and downslope piles recording values of 12.29 and 24.96 MN-m, respectively. These values are close approximation to those measured for the upslope and downslope piles during SE2 for UL5. However, the differences between UL5 and UL10 were quite significant during SE1. This illustrates the bending response under the influence of kinematic interaction is not only the function of input motion characteristics but also strongly depends on the sloping inclinations of the ground surface, which may considerably increase the seismic induced moment demands of the pile for a relatively steeper slope. It may be of interest to note the maximum moments received by the upslope and downslope pile started rising post SE2 as shown in Fig. 22(c) and (d) respectively, with higher maximum moments

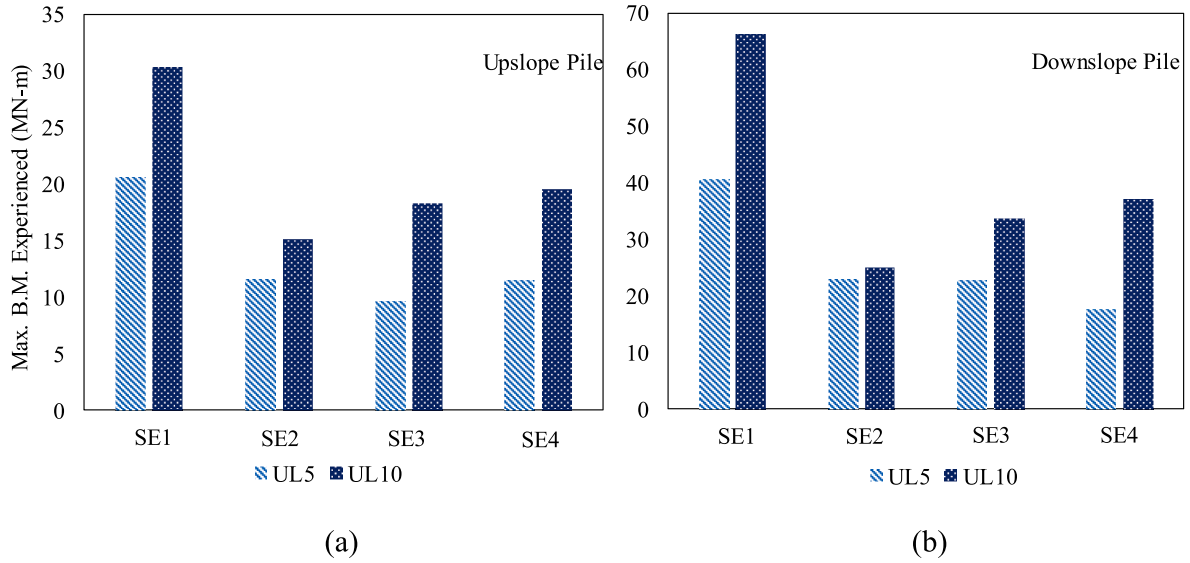

Fig. 23. Comparison of the Max. B.M. during the four S.E. at bottom of the pile (a) Upslope Pile (b) Downslope Pile.

obtained during SE3 and SE4 as compared to SE2. This is in contrast to UL5, where the maximum moments decline post first base excitation.

In the past, some researchers [21] have shown the shadowing effect to be predominant during the lateral spreading, due to which the bending moment arising due to the kinematic interactions might be lesser for the inside (downslope piles), which may be less exposed to the lateral spreading as compared to the upslope pile. However, there are some other studies in the literature (e.g., Ebeido et al. [24], Haskell et al. [39], Kavand et al. [40]), which reported the downslope pile to carry more bending moments during the lateral spreading. The two centrifuge tests (UL5 and UL10) reported in this study also shows the downslope pile to carry significantly larger kinematic moments of considerable higher magnitude during all the shaking events as compared to the upslope pile indicating that shadowing effects may not influence the performance of pile group during the lateral spreading. The reason for the downslope pile carrying significantly larger moments can be explained with the help of observations from the excess pore pressure response (for UL5 and UL10), which showed the upslope side having significantly more dilative spikes as compared to the responses near the piles (which showed considerable less oscillations). Due to this, the downslope pile might not have enough lateral support from the surrounding liquefied soil on the downslope side, which resulted in the downslope pile experiencing significantly larger moments.

Fig. 23 shows the comparison of the maximum moments for UL5 and UL10 during the four shaking events at the bottom of the pile. From the figure, it can be seen that the difference among UL5 and UL10 for both the upslope and downslope pile is considerable during the first base excitation, with significantly larger values obtained during SE1. The reason for the significant moment demands in UL10 as compared to UL5 may be due to the larger magnitude of soil displacement to occur for UL10 as compared to UL5, which might affect soil-pile kinematic interaction.

6. Maximum monotonic bending response of the upslope and downslope piles

Primarily, kinematic response of piles subjected to lateral spreading should be dealt in two different phases which involves consideration of the cyclic ground movement and subsequent lateral spreading of liquefied soil [13]. To study the deformed configuration of the pile system under lateral spreading, it is necessary to remove the cyclic components from the measured kinematic bending response, since lateral spreading is a post liquefaction phenomenon that comprises of the monotonic permanent lateral displacements. A smoothening procedure based on the moving average method was adopted to filter out the cyclic components from the kinematic bending response to obtain the maximum monotonic moments. The maximum monotonic moments were estimated using the incremental approach, where the moments applied for a latter shaking event depend on the previous shaking event. For e.g. the calculation procedure adopted to estimate the maximum monotonic moments for SE4 is explained in equation (2). The soil pressure towards the downslope direction is considered positive in the present study, whereas taken as negative when applied in the opposite direction.

$$M_{F,Max/SE4} = M_{R/SE1} + M_{R/SE2} + M_{R/SE3} + M_{Max/SE4} \quad (2)$$

Where $M_{F,Max/SE4}$ = Final Maximum monotonic moment obtained for SE4.

$M_{R/SE1}$ = Monotonic residual moment obtained for SE1.
$M_{R/SE2}$ = Monotonic residual moment obtained for SE2.
$M_{R/SE3}$ = Monotonic residual moment obtained for SE3.
$M_{Max/SE4}$ = Maximum monotonic moment obtained for SE4.

Fig. 24 shows the maximum monotonic bending moment response for UL5. The maximum moments obtained at the base of the upslope and downslope pile during SE1 are 12.01 and 31.82 MN-m, which predicts larger lateral soil pressures to act on the downslope pile. However, for SE2, the effective maximum monotonic moments reduce to values of 4.08 and 21.46 MN-m, with the soil pressure now acting in the opposite direction. Interestingly, from the SE2 onwards, the maximum moment for the upslope pile at a depth of around 4 m starts increasing, leading to

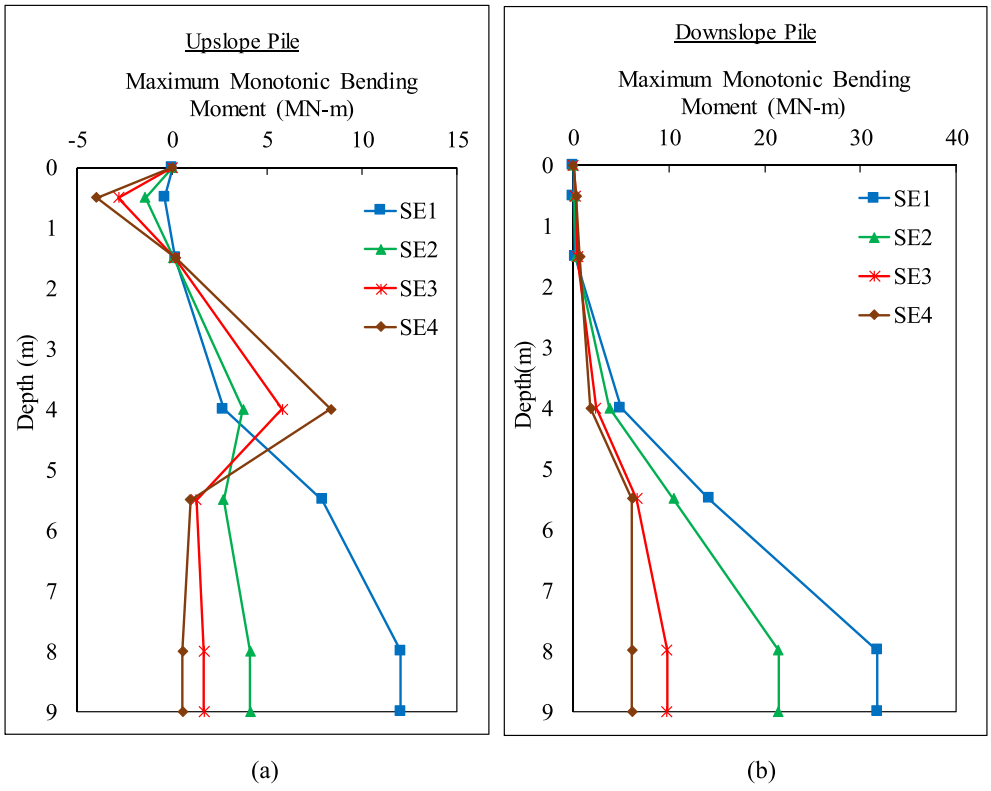

Fig. 24. Maximum Monotonic Bending Moment response of a 2X2 pile group for UL5 (a) Upslope Pile (b) Downslope Pile.

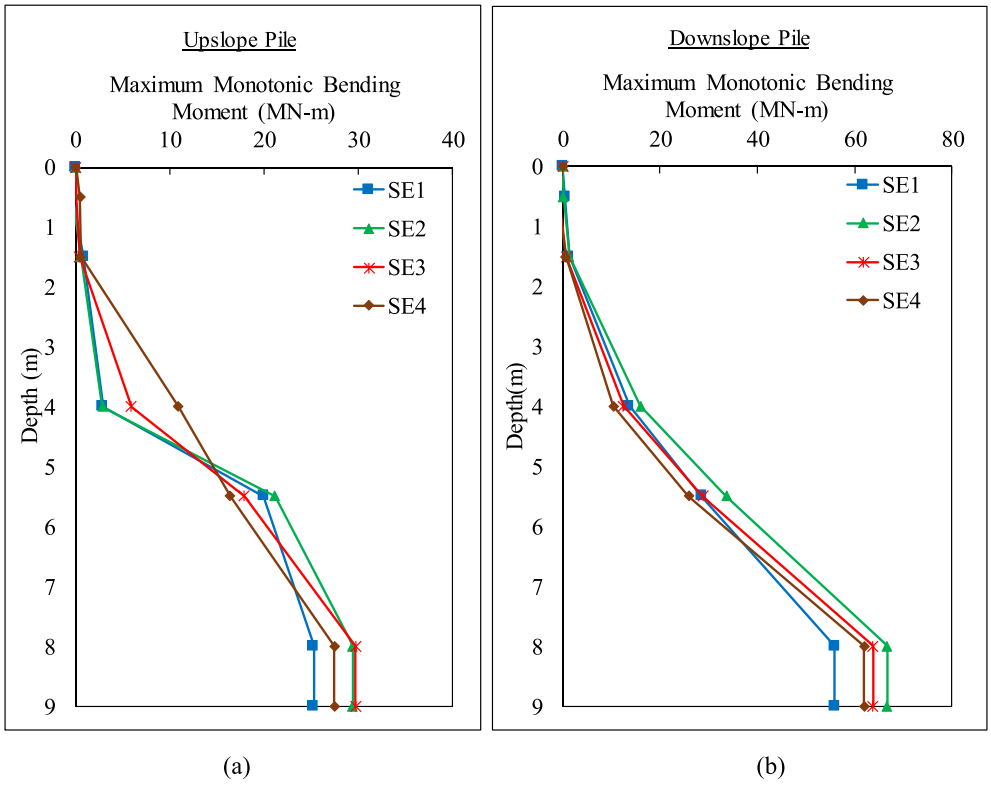

Fig. 25. Maximum Monotonic Bending Moment response of a 2X2 pile group for UL10 (a) Upslope Pile (b) Downslope Pile.

a maximum monotonic moment demand at 4 m along the length of the pile. It is worth mentioning that the moment evaluated at a depth of 4 m at the instance of the upslope pile being subjected to maximum moment is 8.33 MN-m during SE4, which is slightly higher than that recorded for the downslope pile at the base (6.14 MN-m). The downslope pile might bounce back close to its initial position after SE4, with the maximum monotonic moments reducing from 31.82 MN-m to 6.14 MN-m (reduction of 5.18 times) from SE1 to SE4.

Fig. 25 shows the monotonic moment response for UL10 of the pile during all the four SEs. The soil pressure acts in the downslope direction during SE1 with the maximum moment values obtained as 25.72 and 57.19 MN-m, respectively, for the upslope and downslope pile. The max. moment values increase to 30.32 and 68.14 MN-m during SE2 with the soil pressure still acting in the same direction. However, during the latter two shaking events, both the piles tries to bounce back, although the reduction in the maximum moments is not significant as it was for UL5, with the final maximum moments being estimated as 22.22 and 48.57 MN-m, respectively for the upslope and downslope pile.

The Monotonic moment response for UL5 and UL10 represents a complex lateral loading phenomenon under different circumstances, which might lead to different permanent lateral deformations in the piles (post liquefaction) depending on the ground surface sloping, loading intensity which may excite different kinematic interactions among piles with the surrounding liquefiable soil. The results signify the importance of considering the sloping inclination angles of the liquefiable ground surface involving the kinematic interactions of pile, where significantly larger monotonic moments are acting for a relatively steeper slope (UL10) as compared to a gentle slope (UL5). This may lead to piles experiencing larger permanent lateral displacement in UL10. It is worth mentioning that the maximum monotonic moments, experienced by the upslope and downslope pile during SE4 for UL10 is still larger than estimated for the piles during SE1 for UL5.

7. Conclusions

The results from two dynamic centrifuge tests are presented for a 2X2 end-bearing pile foundation in a soil model having different initial ground surface sloping angles subjected to lateral spreading involving four earthquake excitations having an incremental amplitude of shaking. Following conclusions can be derived from the present study:

- Predominant unsymmetrical shear-induced dilative spikes were observed in acceleration data (in the center array of soil model) for UL5. On the contrary, the acceleration data from the UL10 test showed the absence of shear-induced dilative spikes.
- Excess pore pressure response indicated the upslope side to have more pronounced shear-induced dilative spikes as compared with the measured response in the center array. The oscillations were of significantly larger magnitude in the upslope side of UL10 as compared to UL5 during all the shakings throughout the depth.
- The influence of the generated E.P.W.P on the maximum kinematic moment response was studied and it was found the upslope and downslope piles may experience maximum kinematic moments around the onset of liquefaction to the time of initiation of dissipation of excess pore pressure during SE1, when the lateral spreading is predominant (which is also found to depend on the sloping inclination of the ground surface). However, with the increase in intensity of shaking, the maximum kinematic moment may develop well before the initiation of dissipation phase of E.P.W.P.
- The shadowing effects, which were reported in the previous literature involving the lateral spreading, were found to be non-existent in the present study. The maximum positive moment generated on the downslope pile was higher by a factor of 1.97 times in the UL5 test and 2.18 times in the UL10 test as compared to the upslope pile during the first shaking, the responsible physical mechanism is discussed. The configuration adopted for the piles (i.e. fixed end conditions) to simulate the end bearing piles socketed in deep non-liquefiable layer may also be responsible for downslope pile to carry larger moment demands than the upslope pile.
- The present study highlights the importance of consideration of the ground surface sloping angle, with significantly larger kinematic moments being generated for UL10 (both the upslope and downslope pile) as compared to UL5. The maximum positive moment in the upslope and downslope pile was higher by a factor of 1.47 and 1.63, respectively, for UL10 as compared to UL5, the responsible physical mechanism is discussed.
- The largest kinematic moments were generated during the first shaking event for both UL5 and UL10 (for both upslope and downslope pile). However, these moments were significantly lesser during the last three shakings even though the magnitude of base excitations was considerably higher. Larger monotonic moments were also recorded during the first shaking, which is found to depend on the soil lateral displacement; where the monotonic soil displacement reduced after the first shaking. The bottom section of soil model experiencing soil liquefaction rather quickly and for a prolonged time under the higher magnitude of base excitation may also be responsible for the reductions observed in kinematic moments. This may also be due to the transformation of initial sloping ground model into a plainer ground model.

CRediT authorship contribution statement

Anurag Sahare: Conceptualization, Centrifuge Experiments, Methodology, Data analysis, Formal analysis, Investigation, Writing – original draft, Visualization, Revisions. **Kyohei Ueda:** Resources, Writing – review & editing, Supervision. **Ryosuke Uzuoka:** Resources, Supervision.

Declaration of competing interest

The authors declare that they have no known competing financial interests or personal relationships that could have appeared to influence the work reported in this paper.

Acknowledgements

This paper is based on the achievements of the collaborative research program (2021W-03) of the Disaster Prevention Research Institute of Kyoto University. The authors would like to thank Ms. Ayako Namigishi (Lab Technician) at the DPRI centrifuge facility for her help in conducting the centrifuge experiments. The first author would like to thank the Japanese Government for financially assisting his PhD studies with the MEXT scholarship.

Appendix A

Figs. A1 and A2 presents the maximum lateral soil displacement (including cyclic components) at different locations within a soil model for UL5 and UL10. Apart from the laser sensors, the soil displacements were obtained from the accelerometers after double integrations. Larger soil displacements are found to occur at the ground surface near the center array as compared to the downslope side for UL5 as shown in Fig. A1. On the other hand, larger soil displacements are recorded near the downslope side for UL10 as compared to UL5 (Fig. A2), indicating the soil lateral displacements

to depend on the initial sloping inclinations of the ground surface.

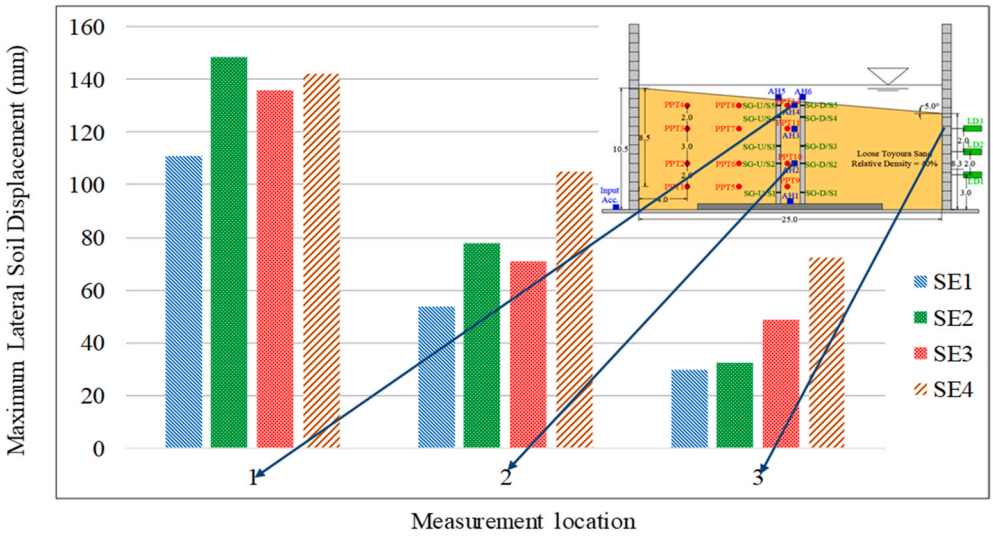

Fig. A1. Lateral soil displacement along the soil model-UL5.

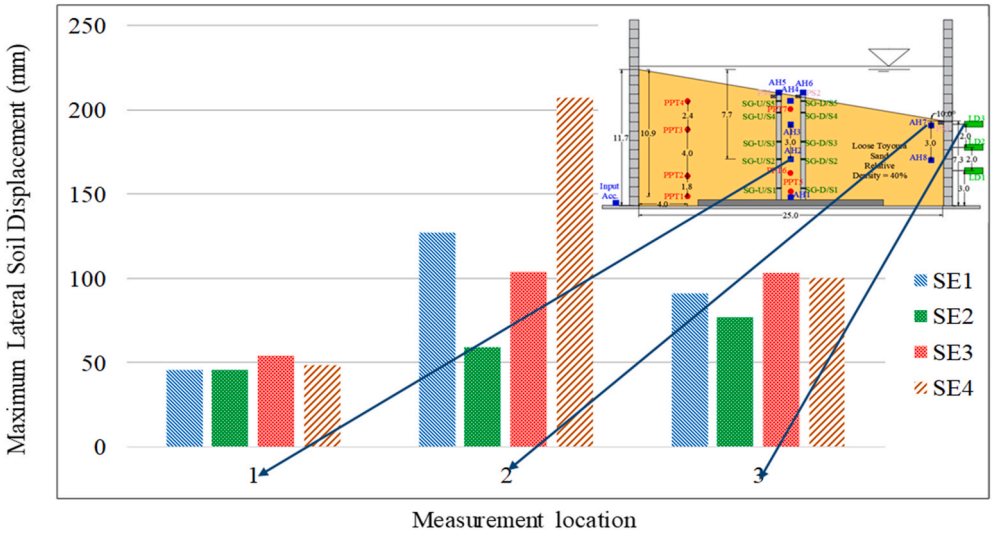

Fig. A2. Lateral soil displacement along the soil model-UL10.

References

[1] Zeghal M, Elgamal AW. Analysis of site liquefaction using earthquake records. J. Geotech. Eng. 1994;120(6):996–1017.

[2] Elgamal A, Zeghal M, Taboada V, Dobry R. Analysis of site liquefaction and lateral spreading using centrifuge testing records. Soils Found 1996;36(2):111–21.

[3] Dobry R, Thevanayagam S, Medina C, Bethapudi R, Elgamal A, Bennerr V, et al. Mechanics of lateral spreading observed in a full-scale shake test. J Geotech Geoenviron Eng 2010;137(2):115–29.

[4] Manzari MT, Ghoraiby M El, Kutter BL, Zeghal M, Abdoun T, Arduino P, et al. Liquefaction experiment and analysis projects (LEAP): summary of observations from the planning phase. Soil Dynam Earthq Eng 2018;113:714–43.

[5] Korre E, Abdoun T, Zeghal M. Liquefaction of a sloping deposit: LEAP-2017 centrifuge tests at Rensselaer Polytechnic Institute. Soil Dynam Earthq Eng 2020; 134:106152.

[6] Sahare A, Ueda K, Uzuoka R. Sensitivity and numerical analysis using strain space multiple mechanism model for a liquefiable sloping ground. In: Geo-congress 2020. ASCE: Geotechnical Earthquake Engineering and Special Topics; 2020. p. 51–9.

[7] Sahare A, Tanaka Y, Ueda K. Numerical study on the effect of rotation radius of geotechnical centrifuge on the dynamic behavior of liquefiable sloping ground. Soil Dynam Earthq Eng 2020;138:106339.

[8] He B, Zhang J-M, Li W, Wang R. Numerical analysis of LEAP centrifuge tests on sloping liquefiable ground: influence of dilatancy and post-liquefaction shear deformation. Soil Dynam Earthq Eng 2020;137:106288.

[9] Vargas R, Ueda K, Tobita T. Centrifuge modeling of the dynamic response of a sloping ground – LEAP-UCD-2017 and LEAP-ASIA-2019 tests at Kyoto University. Soil Dynam Earthq Eng 2021;140:106472.

[10] Hamada M. Large ground deformations and their effects on lifelines: 1964 Niigata earthquake. Technical Report Buffalo. NY: National Center for Earthquake Engineering Research; 1992. Report No.: NCEER-92-0001.

[11] Ishihara K. Terzaghi oration: geotechnical aspects of the 1995 Kobe earthquake. In: Proc., int. Conf. On soil mechanics and foundation engineering-international society for soil mechanics and foundation engineering. Rotterdam, Netherlands: A. A. Balkema; 1997.

[12] Tokimatsu K, Asaka Y. Effects of Liquefaction-induced ground displacements on pile performance in the 1995 Hyogoken-Nambu earthquake. Soils Found 1998;38: 163–77.

[13] Ishihara K, Cubrinovski M. Case studies on pile foundations undergoing lateral spreading in liquefied deposits. In Proc., 5th int. Conf. On case histories in geotechnical engineering 2004. New York: University of Missouri-Rolla.

[14] Cubrinovski M, Winkley A, Haskell J, Palermo A, Wotherspoon L, Robinson K, et al. Spreading-Induced damage to short-span bridges in Christchurch, New Zealand. Earthq Spectra 2014;30:57–83.

[15] Fujii S, Isemoto N, Satou Y, Kaneko O, Funahara H, Arai T, et al. Investigation and analysis of a pile foundation damaged by liquefaction during the 1995 Hyogoken-Nambu earthquake. In: Soils and foundations, special issue on geotechnical aspects of the january 17, 1995 hyogoken-nambu earthquake. vol. 2; 1998. p. 179–92.

[16] Uzuoka R, Sento N, Yashima A, Zhang F. Three-dimensional effective stress analysis of a damaged group-pile foundation adjacent to a quay wall. J Jpn Assoc Earthquake Eng 2002;2(2):1–14 [in Japanese].
[17] Abdoun T, Dobry R, O'Rourke T, Goh SH. Pile response to lateral spreads: centrifuge modeling. J Geotech Geoenviron Eng 2003;129(10):869–78.
[18] Uzuoka R, Sento N, Kazama M, Zhang F, Yashima A, Oka F. Three-dimensional numerical simulation of earthquake damage to group-piles in a liquefied ground. Soil Dynam Earthq Eng 2007;27. 395-13.
[19] Motamed R, Towhata I. Shaking table model tests on pile groups behind quay walls subjected to lateral spreading. J Geotech Geoenviron Eng 2010;136(3):477–89.
[20] Motamed R, Sesov V, Towhata I, Anh NT. Experimental modeling of large pile groups in sloping ground subjected to liquefaction-induced lateral flow: 1-G shaking table tests. Soils Found 2010;50(2):261–79.
[21] Haeri SM, Kavand A, Rahmani I, Torabi H. Response of a group of piles to liquefaction-induced lateral spreading by large scale shake table testing. Soil Dynam Earthq Eng 2012;38:25–45.
[22] Motamed R, Towhata I, Honda T, Tabata K, Abe A. Pile group response to liquefaction-induced lateral spreading: E-Defense large shake table test. Soil Dynam Earthq Eng 2013;51:35–46.
[23] Liu X, Wang R, Zhang JM. Centrifuge shaking table tests on 4 X 4 pile groups in liquefiable ground. Acta Geotechnica 2018;13:1405–18.
[24] Ebeido A, Elgamal A, Tokimatsu K, Abe A. Pile and pile-group response to liquefaction-induced lateral spreading in four large-scale shake-table experiments. J Geotech Geoenviron Eng 2019;145(10):04019080.
[25] Xu Chengshun, Dou P, Du X, El Naggar MH, Miyajima M, Chen S. Seismic performance of pile group-structure system in liquefiable and non-liquefiable soil from large-scale shake table tests. Soil Dynam Earthq Eng 2020;138:106299.
[26] Barlett SF, Youd TL. Empirical analysis of horizontal ground displacement generated by liquefaction-induced lateral spreads. Technical Report Buffalo. NY: National Center for Earthquake Engineering Research; 1992. Report No.: NCEER-92-0021.
[27] Youd TL, Hansen CB, Bartlett SF. Revised multilinear regression equations for prediction of lateral spread displacement. J Geotech Geoenviron Eng 2002;128 (12):1007–17.
[28] Gillins DT, Bartlett SF. Multilinear regression equations for predicting lateral spread displacement from soil type and cone penetration test data. J Geotech Geoenviron Eng 2014;140(4):04013047.
[29] Tobita T, Manzari MT, Ozutsumi O, Ueda K, Uzuoka R, Iai S. Benchmark centrifuge tests and analysis of liquefaction-induced lateral spreading during earthquake. In: Geotechnics for catastrophic flooding events. CRC press/Balkema (Taylor & Francis Group; 2014. p. 127–82.
[30] Bai K, Tobita T, Ueda K, Iai S. New modelling of models for centrifuge model testing. Shanghai, China: Second Asian Conference on physical modeling in Geotechnics; 2016. p. 146–51.
[31] Ueda K, Sawada K, Wada T, Tobita T, Iai S. Applicability of the generalized scaling law to a pile-inclined ground system subject to liquefaction-induced lateral spreading. Soils Found 2019;59:1260–79.
[32] Koseki J, Yoshida T, Sato T. Liquefaction properties of toyoura sand in cyclic torsional shear tests under low confining stress. Soils Found 2005;45(5):103–13.
[33] Brandenberg SJ, Boulanger RW, Kutter BL, Chang D. Behavior of pile foundations in laterally spreading ground during centrifuge tests. J Geotech Geoenviron Eng 2005;131(11):1378–91.
[34] Iai S, Morita T, Kameoka T, Matsunaga Y, Abiko K. Response of a dense sand deposit during 1993 KUSHIRO-OKI earthquake. Soils Found 1995;35(1):115–31.
[35] Elgamal A, Yang Z, Parra E. Computational modeling of cyclic mobility and post-liquefaction site response. Soil Dynam Earthq Eng 2002;22(4):259–71.
[36] González L, Abdoun T, Dobry R. Effect of soil permeability on centrifuge modeling of pile response to lateral spreading. J Geotech Geoenviron Eng 2009;135(1): 62–73.
[37] Chaloulos YK, Bouckovalas GD, Karamitros DK. Analysis of liquefaction effects on ultimate pile reaction to lateral spreading. J Geotech Geoenviron Eng 2014;140(3): 04013035.
[38] Chaloulos YK, Bouckovalas GD, Karamitros DK. Pile response in submerged lateral spreads: common pitfalls of numerical and physical modeling techniques. Soil Dynam Earthq Eng 2013;55:275–87.
[39] Haskell J, Madabhushi G, Cubrinovski M. Effect of pile spacing on the behavior of a pile group in laterally spreading soil. Santiago, Chile: 5th International Conference on Earthquake Geotechnical Engineering; 2011.
[40] Kavand A, Haeri SM, Raisianzadeh J, Meibodi AS, Soltani SA. Seismic behavior of a dolphin-type berth subjected to liquefaction induced lateral spreading: 1g large scale shake table testing and numerical simulations. Soil Dynam Earthq Eng 2021; 140:106450.

Update

Soil Dynamics and Earthquake Engineering

Volume 156, Issue , May 2022, Page

DOI: https://doi.org/10.1016/j.soildyn.2022.107208

Soil Dynamics and Earthquake Engineering 156 (2022) 107208

Contents lists available at ScienceDirect

Soil Dynamics and Earthquake Engineering

journal homepage: www.elsevier.com/locate/soildyn

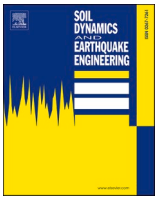

Corrigendum to "Influence of the sloping ground conditions and the subsequent shaking events on the pile group response subjected to kinematic interactions for a liquefiable sloping ground"[Soil Dyn. Earthq. Eng. 152 (2022) 107036]

Anurag Sahare [a,*], Kyohei Ueda [b], Ryosuke Uzuoka [b]

[a] Graduate School of Engineering, Kyoto University, Kyoto Daigaku-katsura, Nishikyo-ku, Kyoto, 615-8530, Japan
[b] Disaster Prevention Research Institute, Kyoto University, Gokasyo, Uji, Kyoto, 611-0011, Japan

The authors regret that they have noticed two required corrections in the original paper.

1. From Figs. 19–25, the bending moment axis title should read as (MN-m) X 10^{-2}.
2. In sections 5 & 6; the bending moments values, which are written in few places should be multiplied by 10^{-2}.

None of these corrections affects any of the discussions made in the original paper.

The authors would like to apologise for any inconvenience caused.

DOI of original article: https://doi.org/10.1016/j.soildyn.2021.107036.
* Corresponding author.
E-mail address: sahare.anuragrahul.4m@kyoto-u.ac.jp (A. Sahare).

https://doi.org/10.1016/j.soildyn.2022.107208

Available online 1 March 2022